

Review

On Defect Minimization Caused by Oxide Phase Formation in Laser Powder Bed Fusion

Anna A. Okunkova *, Semen R. Shekhtman, Alexander S. Metel , Nadegda A. Suhova, Sergey V. Fedorov, Marina A. Volosova and Sergey N. Grigoriev 

Department of High-Efficiency Processing Technologies, Moscow State University of Technology STANKIN, 127055 Moscow, Russia; s.shekhtman@stankin.ru (S.R.S.); a.metel@stankin.ru (A.S.M.); n.suhova@stankin.ru (N.A.S.); sv.fedorov@stankin.ru (S.V.F.); m.volosova@stankin.ru (M.A.V.); s.grigoriev@stankin.ru (S.N.G.)

* Correspondence: a.okunkova@stankin.ru; Tel.: +7-909-913-12-07

Abstract: The article is devoted to the compressive review of the defects observed in the products of the machinery usage made mainly of anti-corrosion steels of the martensite-austenite group, difficult to process materials such as pure titanium, nickel, and their alloys, super and high entropy alloys and triple fusions produced by laser additive manufacturing, particularly the laser powder bed fusion. Studies were conducted on the structural defects observed in such products to improve their quality in the context of residual stress elimination, porosity reduction, and surface roughness improvement. Electrophysical and electrochemical treatment methods of removing oxide phase formation during melting and remelting of deposited tracks in layers are considered (such as ultrasound, plasma, laser, spark treatment, induction cleaning, redox annealing, gas-flame, plasma-beam, plasma-spark treatment). Types of pollution (physical and chemical) and cleaning methods, particularly plasma-based methods for oxide phase removing, are classified. A compressive comparison of low- and high-pressure plasma sources is provided. Special attention is focused on the atmospheric plasma sources based on a dielectric barrier and other discharges as a part of a production setup that presents the critical value of the conducted review in the context of the novelty for transition to the sixth technology paradigm associated with the Kondratieff's waves.

Keywords: surface cleaning; laser powder bed fusion; selective laser melting; atmospheric plasma sources; dielectric barrier discharge; nickel alloy; titanium alloy; anticorrosion steel



Citation: Okunkova, A.A.; Shekhtman, S.R.; Metel, A.S.; Suhova, N.A.; Fedorov, S.V.; Volosova, M.A.; Grigoriev, S.N. On Defect Minimization Caused by Oxide Phase Formation in Laser Powder Bed Fusion. *Metals* **2022**, *12*, 760. <https://doi.org/10.3390/met12050760>

Academic Editors: Atef Saad Hamada and Pasquale Cavaliere

Received: 22 February 2022

Accepted: 19 April 2022

Published: 28 April 2022

Publisher's Note: MDPI stays neutral with regard to jurisdictional claims in published maps and institutional affiliations.



Copyright: © 2022 by the authors. Licensee MDPI, Basel, Switzerland. This article is an open access article distributed under the terms and conditions of the Creative Commons Attribution (CC BY) license (<https://creativecommons.org/licenses/by/4.0/>).

1. Introduction

Additive technologies for the production of products are the primary trend of recent years in power engineering, automotive, mechanical engineering, biomedical engineering, aerospace, and defense industries [1–4]. Additive technologies fundamentally change the production process by layer-by-layer growing solid according to a digital 3D model [5–9]. The introduction of additive technologies provides ample opportunities to manufacture complex profile products with high accuracy, up to ± 0.05 mm, depending on the used modes [10–12]. The technology also allows working with non-standard materials up to oxide ceramics and glasses [13–15] and using the technology as thermal post-processing of three-dimensional complex-shaped products made by other methods [16].

Increasing additive production's mobility and flexibility have modified the digital system of technological production preparation. It has moved it into a virtual environment allowing a quick transition to the production of new products without developing the specific technological documentation and tooling for each specific product that usually hampers rapid technical preparation for the production of new products in a short time (work preparation process can be reduced from traditional 6–12 to 1–2 months for engineering products) [17,18]. Digitalizing the production causes traditionally as well the ability to reduce the impact of the human factor on the quality of the resulting products [19] and

reduce the duration of design and technological preparation on extra tooling of the first and second order (for example, stamps and dies and profile cutters for their production) [20,21].

The possibility of manufacturing parts that are not inferior and sometimes even exceed the physical and mechanical properties of parts obtained by traditional methods can be named as one of the known advantages that extends the product's life in the conditions of extreme exploitation (cyclic thermal or mechanical loads) [22,23]. An ability to manufacture parts of complex configurations with internal structures from bimetals makes additive manufacturing outstanding from traditional shaping [24,25] and allows reducing the grown object weight by internal cavities forming. High material utilization rate due to the production of workpieces with a minimum allowance for subsequent machining and the recovery of up to 99% of uncured material for reuse in the production cycle increases production efficiency [26]. However, it should be noted that implementing traditional machining methods leads to the loss of raw materials that can reach up to 80–85% in the production of dies for injection molds that require the massive volume milling of the internal cavity of workpieces [27].

Among the most striking shortcomings, scientists identify the high costs for equipment and electric power, powder material of specific parameters, insufficient rates of newly developed material introduction, and the inability of quick technology adoption for these materials in place [4,28,29]. Among others, it can be named high post-processing costs for small production volumes and relatively low productivity for growing large-sized solids (with overall dimensions of more than 100 mm can take up to a few days) [30]. Growing large-sized parts is also associated with a deviation in accuracy that grows from the centrum of the part profile in plane to its periphery. The shape of the laser beam spot is an axisymmetric circle closer to the center when it looks like an ellipse-shaped with a more blurred edge closer to the periphery that is especially noticeable on the parts with an overall size of more than 300 mm in-plane [31,32]. Insufficient quality of single-track formation influences the quality of the part dramatically and leads to the deviations of the grown solid [33,34].

Another known advantage is that powder material reusing leads to deterioration of powder properties during re-exploitation due to the energy excess in the melt pool, ejecting partly fused particles out of the processing area [35,36]. The absence of scientifically based recommendations on the choice of LPBF factors for producing the parts from known but still not adopted for LPBF specifics steels and alloys, non-standard alloys, new metal-based materials, superalloys, high-entropy alloys, triple fusions, etc. can hampers development of the technology and transition to the next technological paradigm [37–40].

Despite all mentioned shortcomings, LPBF is considered economically feasible when shaping is impossible by traditional methods and when time on tooling production slows down the production of a prototype, and also in the case of the low utilization rate of high-cost processed materials and the production of high-tech, small-scale or personalized products [41–43] made of a broad range of engineering materials (Table 1).

Table 1. The most spread engineering materials for LPBF.

| Material | References |
|--|------------|
| Technical ceramics | [44] |
| Tool steels | [45] |
| Anti-corrosion steels | [46,47] |
| Gradient materials (anti-corrosion steel/carbides of the group 4, 5 and 6 transition metals (with the exception of chromium) | [48] |
| Al and Al-based alloys | [1,23,49] |
| Ni and Ti alloys | [50,51] |
| CoCr alloys | [52,53] |
| High reflective and thermo conductive metals and alloys of the copper subgroup | [54,55] |

LPBF is used in industry to produce complex-profile parts of assembly units and assemblies, non-separable multi-element assemblies [56], dies and mold parts [57], forming inserts for chill casting [58], a wide range of engineering scaffolds [59,60].

Formed solidification defects include discontinuities and microstructural imperfections in the fabricated components that are still inevitable [61,62]. The study of the grown material defects showed the formation of such defects as intertrack lack of fusions, localized brittle zones, and grain coarsening in the heat-affected zones, leading to anisotropic ductility behavior along with layer deposition and growing solid directions. This review paper provides the associated defects of grown material structures and summarizes technologies of surface cleaning being deployed to mitigate the defects such as residual stresses, pores, oxide phase formation, and improving surface roughness.

The work is mainly devoted to the production of engineering products produced of a wide range of metallic materials to reduce their labor intensity and, in prospect, enlarge their exploitation properties for working in cyclic loads, in particularly:

- a quarter-turn lock mechanism of the aircraft that includes a pin, washer, and sleeve made of X20Cr13 (AISI 420) steel with a diameter of 11 mm, a height of 7 mm, complex-shaped, where the traditional technology is rather laborious and complicated;
- an air intake grille module made of X10CrNiTi18-10 (AISI 321) steel, which is an element for protecting the air intake duct from the objects entering it and is an obstacle to the air intake to the engine with overall dimensions of 180 mm × 100 mm × 30 mm with the minimum thickness of the inclined by 0.5–1.0° walls of 0.3 mm; traditionally the module is characterized by high labor intensity, including following operational steps such as cutting, bending, manual assembly of almost seventy parts, welding, and soldering.

The material of the washer should be wear-resistant, the material of which should differ in strength from the lock pin material by 20%, where the strength is not less than 1300 MPa, hardness is not less than 42 HRC, the density is not less than 7.7 g·cm⁻³, arithmetic mean deviation R_a is less than 3.2 μm. Another airplane part should be produced with tensile strength not less than a standard semi-finished product with a density of less than 7.9 g·cm⁻³, and arithmetic mean deviation R_a of less than 6.3 μm. LPBF of these parts takes the production to a new level [63–65].

Therefore, the task of studying the relationship between the LPBF factors and their influence on fused material structural defects, understanding the mechanism of defect formation, design and development of the specific atmospheric plasma source based on a dielectric barrier discharge for LPBF product surface cleaning is relevant.

The following tasks are defined to achieve minimizing structural defects of LPBF products:

- Study the formation mechanism of an undesirable oxide phase (defects);
- Conduct analysis of methods for removing the oxide phase by atmospheric plasma sources from the surface after exposure to a laser beam;
- Highlight and systematize an atmospheric plasma source principles based on the dielectric barrier and other discharges as part of a technological installation.

2. Study of Formation Mechanism of Oxide Phase (Defects)

2.1. Study of the Effect of Process Parameters on Defects in LPBF

Currently, additive technologies are implemented based on light-beam and electron-beam energy sources. However, today's most popular additive technologies based on laser radiation are related to melting, sintering, and direct metal sintering principles. When implementing the technology of selective laser sintering, the compaction of the layer of powder material occurs due to solid-phase sintering. In the basis of direct laser sintering of metals, densification occurs according to the mechanism of liquid-phase sintering due to the melting of a fusible component in a powder mixture. In the basis of the laser powder bed fusion method, the compaction of the powder material is carried out due to the complete melting and spreading of the melt. The structure of the product obtained by selective laser melting is shown in Figure 1 based on some findings in [33,34].

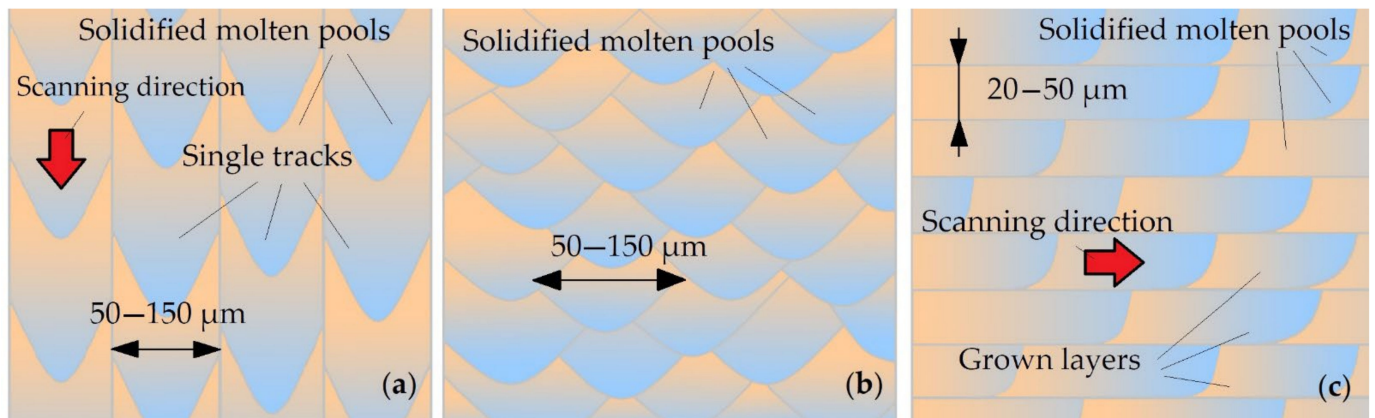


Figure 1. The schematic structure of the metal product obtained by LPBF: (a) Top view; (b) Cross section; (c) Longitudinal section.

Obtaining a surface of the required quality is one of the most critical issues of LPBF. However, the lack of data on the modes of laser powder melting and the powder materials themselves necessitates multiple research projects in this area [66–72]. The LPBF process is multifactorial, and a whole set of factors influences the formation of defects [33,34,71].

Further improvement of additive installations is associated with using a more powerful laser generator, a smaller diameter of the focusing spot, and a thinner layer of powder, which made it possible to use LPBF to obtain products from various metals and alloys of the required quality level.

With LPBF materials such as aluminum and copper subgroup, an important issue is their high reflectivity [1,23,49,54,55], which determines the need for a powerful laser system. However, increasing the power of the laser beam can adversely affect the dimensional accuracy of the product because if heated excessively, the powder material will melt and sinter outside the laser spot due to heat transfer. In addition, the high power of the laser generator can lead to a change in the chemical composition because of metal evaporation, which is typical for alloys containing low-melting components and having high vapor pressure.

One of the important conditions in the implementation of the LPBF is creating a protective environment that prevents the oxidation of the powder. The composition of the gaseous medium in the working chamber is an important technological parameter of the LPBF. It is known that the absorption of atmospheric gases during metal melting negatively affects its physical and mechanical properties. Therefore, a protective environment of inert gases (N_2 or Ar) is created and maintained in the working chamber. However, inert nitrogen gas as a shielding gas is limited because nitrides may form (e.g., AlN, TiN in the manufacture of aluminum and titanium alloy products), which leads to a decrease in the material's ductility. Furthermore, it has been established that the flow rate of the working gas and the direction of its flows affect the degree of porosity in titanium alloys synthesized using the LPBF technology due to the possible transfer of oxide inclusions formed during powder melting to the scanning zone [1,23,51,73,74].

Practice shows that working with technologically difficult materials such as titanium and nickel alloys leads to the formation of residual stresses, leading to warping of parts and even cracks [50,51,75,76]. Compared with stainless steel, aluminum powders have a higher powder reflectivity (over 91% for aluminum) for laser radiation and higher thermal conductivity, making the process more difficult. Oxide formation on particles when using aluminum powders can lead to defects due to the ingress of oxide films into the alloy since aluminum oxide has a higher melting point (2072 °C) than pure metal (660.3 °C). The upper oxide film from the melt pool evaporates under the action of the laser beam, whereas the oxide films located deeper in the melt are untouched and remain inside, representing defective zones. Finally, the hydrogen content of the powder can cause pores in the part if the melt pool crystallizes faster than the gas evaporates.

The quality of powder materials is characterized by granulomorphometric properties (sphericity, dispersion), geometric dimensions, and physicochemical characteristics. The study of the effect of particle size on the properties of finished products showed that in order to obtain high-quality products without porosity, the presence of small particles is necessary. During laser exposure, small particles are first melted, thereby creating favorable conditions for melting larger particles. In addition, the spherical particles improve the fluidity of the powder and can be packed more densely. A wide particle size distribution allows for a denser arrangement of particles. A uniform layer is formed with sufficient fluidity of the powder. The size distribution of particles affects the mode factors that differ for large and small particles.

An important characteristic of powders is also the structure of their constituent particles, which can be both compact and porous. In this case, the pores can access the surface (open porosity) or be closed inside the particle (closed porosity).

Used metal powders must meet the following requirements [77,78]:

- homogeneous chemical composition;
- sphericity of powder particles with a shape factor from 1.0 to 2.0 (sphericity guarantees high fluidity and packing density, which leads to rapid and reproducible distribution of powder layers);
- a narrow and uniform range of particle size distribution with an average value of 40 to 75 μm (the content of particles whose size is larger than the allowable or irregularly shaped particles can cause defects in the finished part).

Powders that meet these requirements have:

- Low coefficient of friction between particles;
- Satisfactory fluidity;
- Increased bulk density;
- Satisfactory density after shaking.

Such requirements allow uninterrupted powder supply and its deposition in thin layers in the LPBF. Depending on the required level of quality, appropriate post-processing is required [79–81].

The multifactorial nature of the LPBF, the need to determine the optimal modes of formation of products of the established quality level, and when using new alloys and materials hinder the widespread use of this method. Quality management of products obtained by LPBF technology is based on understanding the mechanism of defect formation.

2.2. Study of the Mechanism of Formation of Structural and Surface Defects

An analysis of the literature sources has shown that, to date, studies of the quantitative correlation of the formation of defects with process parameters are of a disparate nature. The main defects of LPBF technology include cracks, delamination of parts/cracking and warping, porosity, the density of the part, reduced plasticity due to the presence of residual stresses, surface roughness (Table 2). The table is suitable for nickel and titanium alloys (including high-entropy alloys), anti-corrosion steels of the martensite-austenite class, and some oxide ceramics suitable for LPBF.

Table 2. Defects in laser powder bed fusion.

| Defects | Possible Reasons | Solutions | References |
|---|--|--|---------------------|
| Cracks (surface, internal, through) | <ul style="list-style-type: none"> • Too high mode than required (especially it is actual for newly introduced metals and alloys or difficult-to-process materials and alloys of nickel-titanium group, and high-entropy alloys), • Powder quality, • Residual stresses | <ul style="list-style-type: none"> • Use of supporting structures for fast and efficient heat dissipation; • Optimal orientation of parts in the build chamber to reduce the area of welded sections; • Heated build platform, which reduces the temperature gradient and reduces residual stresses; • Chessboard scanning strategy; • To avoid further cracking during operation, heat treatment to relieve internal stresses is recommended, etc. | [14,24,75,76,82,83] |
| Porosity | <ul style="list-style-type: none"> • Too high modes; • Granulomorphometry of the powder (size, sphericity, dispersion of the powder); • The oxide film present on the surface of the powder particles; • Layer deposition density; • Shrinkage processes, capture of molecules (nitrogen, argon) during synthesis | <ul style="list-style-type: none"> • Selection of the optimal LPBF modes (speed, laser radiation power, scanning strategy); • Selection of optimal granulomorphometry (shape, size, dispersion); • Input quality control of powders; • Consistency of the quality level of the used powder; • Carrying out subsequent processing methods, for example, hot isostatic pressing, etc. | [14,30,47,62,84] |
| Increased degree of stress-strain state | <ul style="list-style-type: none"> • Residual stresses; • Product geometry; • Location of supporting structures; • Heating and cooling rates; • Technological heritage; • Chosen material physical properties; • Process parameters (laser power and speed, powder layer thickness, scanning strategy, preheating, etc.) | <ul style="list-style-type: none"> • Selection of the optimal LPBF modes; • Carrying out heat treatment (annealing); • Rescan; • Platform heating | [8,45,72,82] |
| Increased surface roughness | <ul style="list-style-type: none"> • LPBF process modes; • Peculiarities of LPBF (layer-by-layer deposition of the powder material and the formation of steps, which are more pronounced with a significant inclination of the surfaces; • Partial melting of granules from an array of powder outside the shaded section due to partial penetration of the previous deposited layer) | Selection of the optimal LPBF modes (reducing the scanning interval leads to an improvement in surface roughness; reducing the scanning speed reduces coagulation and improves surface roughness) | [8,18,47,82,85] |

Cracks are among the most dangerous mechanical defects in the LPBF [14,86], in which low thermal conductivity and high coefficients of thermal expansion create sufficiently

high internal stresses to break bonds within the material, especially along grain boundaries where dislocations are present.

Several physical phenomena are important to the LPBF, such as the absorption of laser radiation by the powder material, melt droplet coagulation phenomena that disrupt the formation of continuous layers, and thermal fluctuations experienced by the material during the process, which can lead to cracking and damage to the product being grown [8,86].

Cracks can occur due to not using a laser source with sufficient power or too fast scanning of the powder surface, which leads to insufficient metal melting and preventing a strong bonding medium for solidification [87]. Moreover, residual stresses can lead to cracking (a mechanical defect in which low thermal conductivity and high coefficients of thermal expansion create sufficiently high internal stresses to break bonds within the material, especially along grain boundaries where dislocations are present) of parts and their deformation [86]. The value of residual stresses is affected by the product's geometry, the rate of heating and cooling, and the coefficient of thermal expansion, phase and structural changes in the metal. Studies were carried out to assess the residual stresses and strains for various scanning strategies [88]. The maximum stresses along the X and Y axes were observed for samples with a scanning strategy along the contour when shifted to the center. Checkerboard scanning, also known as island scanning, has been proven to reduce residual stresses compared with other scanning strategies using a random sequence of islands.

Secondary effects due to the laser beam can unintentionally affect the properties of the structure. One such example is the formation of secondary phase precipitates in the bulk structure due to repeated heating in the solidified underlying layers as the laser beam passes through the powder layer. Depending on the composition of the precipitates, this effect can remove important elements from the bulk material. In addition, the laser power and convection currents generated in powder layers containing oxides can evaporate and "splatter" the oxides elsewhere. It is typical for the LPBF that the deposited powder is remelted several times during the construction of the product, ensuring reliable adhesion of the formed layers (Figure 2) [8,89].

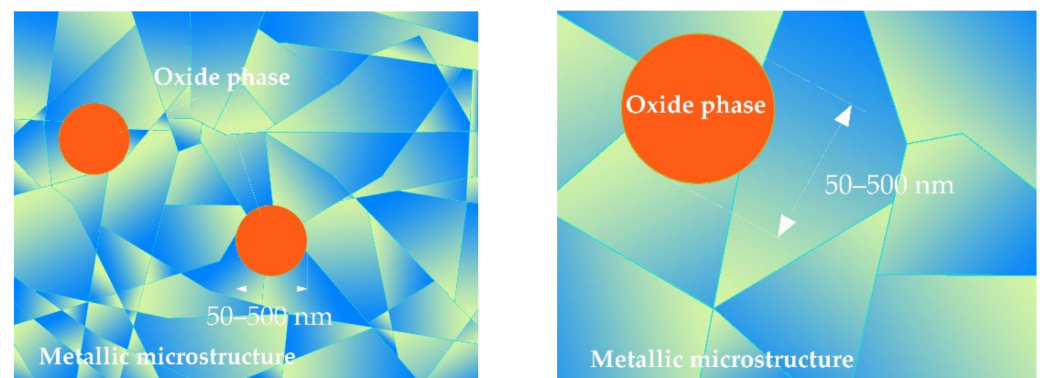


Figure 2. Oxide nanoparticles correspond to a small extent to steel obtained by LPBF.

In this case, the material is heated above the melting point, and a thin oxide film inevitably appears on the deposited surface, despite the fact that the oxygen content in the laser chamber is set to no higher than 0.15%. If this film is not removed, then during the formation of the next layer it will be walled up in the product and during the remelting of the layer formed above the film, it will remain in the structure of the product in the form of spherical nanoparticles of the amorphous oxide phase, evenly distributed over the volume of the product (Figure 2).

These oxides accumulate and do not wet, thereby forming slag, which not only removes the useful nature of the oxide in the composition, but also provides a mechanically favorable microenvironment for material cracking [8,90].

Pore formation is a very important defect in LPBF. Pores are found to form during changes in the laser scanning speed due to the rapid formation and then collapse of deep pits on the surface, which trap the inert shielding gas in the solidifying metal.

The main causes of porosity are incorrect selection of LPBF parameters and powder quality. An increase in the energy density of laser radiation leads to excessive evaporation of the material and the formation of splashes, which leads to an increase in the pore volume [85]. In addition, the high energy density of the laser radiation leads to the formation of a large melt pool, which becomes less stable and leads to the formation of separate melt droplets (balling effect) rather than a continuous melt path. Melt drops, under the action of surface tension, draw in nearby powder particles, which leads to the formation of pits around the drops and, as a result, an increase in porosity [86].

At the same time, when the energy density of laser radiation is insufficient, complete melting of the powder is not ensured, and large pores appear along the scanning lines. The size of the melt pool is too small to be in contact with adjacent scan tracks [34,35,87,91].

The speed of laser scanning affects the type of pores formed during the LPBF [30,33,71,84,85]. The porosity and pore size increase significantly with an increase in the scanning speed.

Insufficient distance between the tracks leads to an increase in porosity in the synthesized products, which is associated with the formation of a non-continuous melt track [34].

The deterioration of the process of spreading and wettability by the melt of the underlying layer is also facilitated by the presence of oxygen, which, dissolving in the metal, increases the viscosity of the melt.

The authors of [82] suggested that the oxide film present on the surface of the powder particles remains in the melt bath, thereby creating residual porosity in the crystallized volumes. The authors of [92,93] showed that the oxide film on the previous layer prevents interlayer bonding and leads to melt droplet coagulation, since metal melts usually do not chemically react with oxide films.

In addition to the LPBF parameters, the appearance of pores is influenced by the quality of the used powder materials, the size and sphericity of the particles, and the granulometric composition's uniformity (dispersity).

The more the shape of the particles approaches a spherical shape, the greater the density of the backfill. Less spherical particles form structures of the second order, which are characterized by large extended pores.

The study of the effect of particle size on the properties of finished products showed that in order to obtain high-quality products without porosity, the presence of small particles is necessary [94]. During laser exposure, small particles are first melted, thereby creating favorable conditions for the melting of larger particles. The presence of particles in the powder, the size of which is larger than the allowable or particles of irregular shape, negatively affects the porosity of the product.

Methods for reducing porosity in LPBF [95,96] include mainly powder quality control (granulomorphology and granulomorphometry, particularly degree of reflection/absorption of laser radiation by the powder), search for the optimal range of process factors, additional methods of leveling/compacting the powder in the layer, pre-drying, leveling the layer, pressing, wetting, pre-heating or heating, pre-melting, subsequent post-processing. The input control of the powder is carried out by assessing the presence of voids and their volume, particle size, shape and linear dimensions, which is important for assessing whether the particle size falls within the desired range.

In addition, subsequent processing methods such as hot isostatic pressing (HIP) can reduce porosity [97]. The use of HIP makes it possible to eliminate residual porosity and improve the physical and mechanical properties of the material.

After additive manufacturing by the LPBF, materials are characterized by anisotropy of properties, increased strength and reduced ductility due to the presence of residual stresses [8,86,97]. Annealing is carried out to remove residual stresses, obtain a more balanced structure, and increase the viscosity and plasticity of the material [98]. Sometimes

remelting or premelting can be used to increase density, reduce residual stresses, etc. [99]. This strategy requires double scanning of the same layer with possibly different parameters without applying powder, although this may increase production time. Platform heating allows reducing the gradient and reducing residual stresses [100].

A checkerboard scanning strategy can also be used to reduce residual stresses in metal parts [94,101]. This strategy works by dividing the scanned area into squares of a given size, which reduces the size of the scanned sections and reduces the length of the scan vector.

However, a team consisting of scientists from the National Institute of Standards and Technology (NIST), Livermore National Laboratory Lawrence (LLNL) and other institutions found that the island scanning method actually increases residual stresses when printing certain bridge-like geometries [102]. Those, the use of the staggered scanning strategy makes it possible to reduce residual stresses, but has restrictions on the geometry of the products. A subsequent heat treatment can be used to relieve internal stresses. The grown parts, fixed by supporting structures on the building platform, are placed in an oven and aged according to the modes [30,47].

The main reason for the increased surface roughness of products obtained by the LPBF method is the way the technology is implemented: layer-by-layer melting of powder material by means of high-power laser radiation. According to the results of studies [103], the roughness of the surface layer is influenced by the parameters of the technological process such as the power of laser radiation, the scanning speed, the layer thickness and the scanning strategy. Surface roughness is directly dependent on technological modes and correlates with the nature of the change in porosity.

It was found that coagulation has a great influence on the roughness of the surface layer. Coagulation is the fusion of small powder particles into larger ones under the influence of laser radiation. A decrease in coagulation was observed with a decrease in the scanning speed, which is due to an increase in the melting time of the powder and a decrease in the viscosity of the melt. Increasing the scanning step leads to an increase in surface roughness. The surface roughness has the smallest value of 15 μm at a laser power of 200 W and a scanning speed of 3000 mm/s. The authors proposed to improve the roughness of the inclined surface due to the contour scanning of each layer with increased energy density [85].

The study of the influence of the quality of the powder material on the roughness showed that the smaller the powder particles, the more accurately it is possible to build products by reducing the scanning step and to obtain a smoother surface by reducing the thickness of the powder layer. However, in the process of product synthesis, a very rapid melting process occurs in the area of the laser spot, accompanied by boiling of the metal with the splashing of the melt and “carrying out” of fine light powder particles from the construction zone, which leads to the formation of an increased roughness of the product [52,53]. This effect can be reduced by using low-power lasers, but this significantly reduces productivity. Subsequently, processing (sandblasting, grinding, and polishing) is used to improve the roughness [30,47].

3. Analysis of Methods for Removing Oxide Phase by Atmospheric Plasma Sources after Laser Treatment

3.1. Investigation of Methods for Removing Oxide Phase

One of the main problems in the selective laser melting of metal powders is the oxide phase. It complicates the LPBF of metal powders and prevents the normal formation of layers during melting.

It is necessary to clean the formed surfaces for the further LPBF carefully to reduce the negative effect of the oxide phase. Mechanical, chemical, electrochemical, physical, thermal, and combined cleaning methods are used to remove the unwanted oxide phase.

Ultrasonic, plasma, laser, spark, induction, gas thermal, and combined methods can be used to remove the unwanted oxide phase in the LPBF operating chamber. A comparative analysis of the methods for oxide phase removal in LPBF is presented in Table 3.

Table 3. Methods for removing the oxide phase.

| Nature | Method | Ability to Clean Complex Shapes | Remarks | Sources |
|----------|-------------------------------------|--|--|-----------|
| Physical | Ultrasound | The need to use special solutions, the need for complex ultrasonic transducers | Exclusion of the use of flammable and toxic solvents | [104,105] |
| | Plasma | Allows you to clean products without the use of heat and the use of special liquid media, allows you to process parts of complex shape does not require Additional resources, cleaning the surface retains its original appearance | Ability to clean geometrically complex objects | [106–108] |
| | Laser | There are restrictions on the thickness of the processed material | Possibility of 100% localization of cleaning products | [109] |
| | Spark | | The complexity of the equipment, causes surface modification | [110] |
| Thermal | Induction cleaning, redox annealing | The technology is effective when using long bars | Possibility of surface overheating, sophisticated equipment and qualified personnel | [111] |
| | Gas-flame | Slight heating of parts, used to clean parts with a thickness of more than 5 mm | The need for subsequent cleaning by mechanical action, combustion products remain on the surface | [112] |
| Combined | Plasma-beam, plasma-spark | Allows processing of complex parts | The complexity of the equipment, the complexity of the implementation process | [113] |

The performed analysis showed that one of the methods that allows to efficiently and effectively remove the oxide phase that occurs during the LPBF, providing conditions for reliable and durable formation of the product, is the plasma method.

3.2. Analysis of Methods for Removing Oxide Phase by Sources of Atmospheric Plasma

Atmospheric pressure plasma is generated at atmospheric pressure without the use of complicated and expensive vacuum equipment. In this regard, atmospheric plasma is one of the promising processing tools in various fields of science and technology. Atmospheric low-temperature plasma and devices based on it, realizing a corona discharge, glow discharge, discharge with a dielectric barrier, and others, are widely used in various technologies [114,115].

Atmospheric plasma can be used to local clean surfaces of various materials such as metals, various types of ceramics, and other temperature-resistant metal- or ceramic-based materials.

The purpose of atmospheric pressure plasma cleaning is to remove contaminants, any substrate, even molecular traces of contaminants that form on the surface. Surface cleaning is the initial step in the surface preparation process. There are two types of pollutants—“natural” and “technological”. Natural effects of the surrounding atmosphere appear, mainly containing oxygen-carbon or carbon-hydrogen bonds of organic substances, oxides, and adsorbed water particles. A technological type of pollution may occur during the part’s manufacturing process.

There is another classification of pollution based on [8,47,82,116–122]. All pollution is divided into physical and chemical ones. Physical pollutions are held on the treated surface due to Van der Waals forces (electrostatically); chemical ones are due to chemical bonds. Different types of contaminants are removed by different methods (Table 4).

Table 4. Pollution classification.

| Type of Pollution | Cleaning Method | References |
|-------------------|-------------------------|-------------|
| Physical | Washing | [116] |
| | Ultrasonic cleaning | [82] |
| | Heat treatment | [47,82] |
| | Plasma cleaning | [8,117,118] |
| Chemical | Processing in solutions | [119] |
| | Acid and alkali etching | [120] |
| | Gas etching | [47] |
| | Laser chemical cleaning | [121,122] |

Surface treatment with plasma flows creates a low-temperature environment by using electrical energy rather than thermal energy to stimulate chemical reactions. The speed of plasma cleaning is not high (~0.4 mm/hour) [123,124]; therefore, plasma cleaning is often used as a finish cleaning, immediately before further processing (for example, coating deposition).

Plasma treatment satisfies the progressiveness criteria (the degree of progress in technology, technological equipment and organizational forms of processes, which includes qualitative and quantitative indicators [125]) such as:

- Low duration of the process;
- High degree of cleanliness of the treated surface;
- Homogeneity of the cleaned surface;
- No changes in the structure of the substrate material;
- Environmental safety;
- The possibility of quick disposal of cleaning products.

During the implementation of plasma surface treatment, electrons, ions, and radicals are generated. The atmospheric pressure plasma flow, interacting with the treated surface, causes the following phenomena leading to effective cleaning: heating of the surface to be cleaned, spraying, and etching. The advantages and disadvantages of these processes are shown in Figure 3.

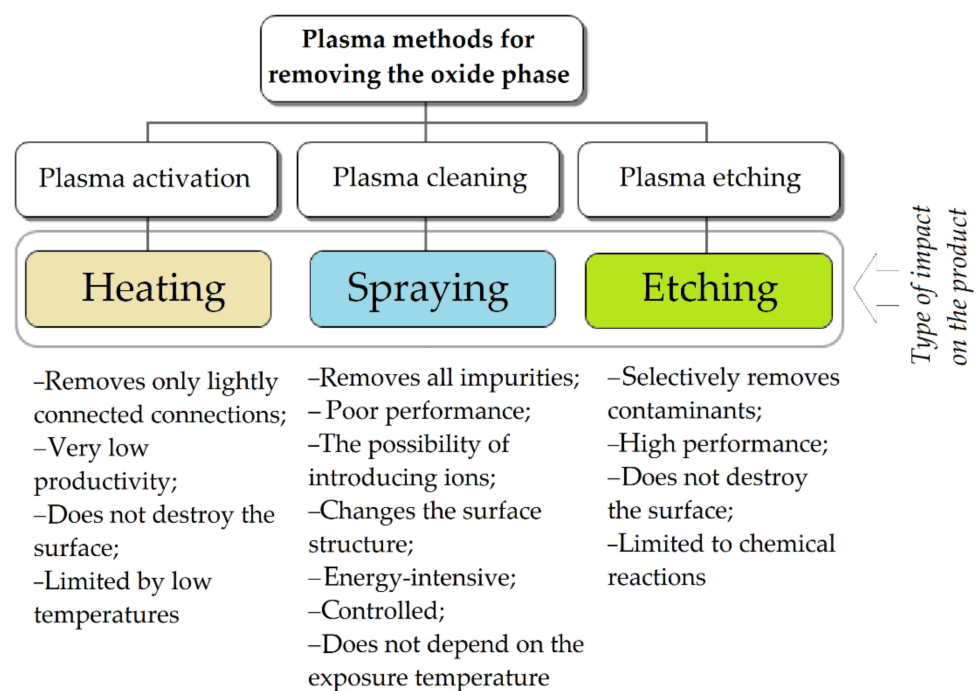


Figure 3. Plasma methods for removing the oxide phase.

Plasma treatment with atmospheric plasma reduces surface contamination by 5–6 times than chemical cleaning methods. Atmospheric plasma cleaning prepares the surface without any harmful waste.

Depending on the design solution and practical implementation of plasma surface treatment in order to clean it from the oxide phase and ensure strength properties, plasma cleaning, plasma activation, and plasma etching are used [126,127] (Figure 3).

When implementing plasma heating to clean the surface, the substrate to be cleaned is heated mainly by bombarding the surface with the electron and ion components of the plasma and by plasma radiation. It is possible to increase the plasma energy flux by applying a bias potential. Surface heating is usually limited to a low temperature (~600 °C) due to the prevention of the formation of metal carbides. At the same time, such a process can remove only lightly bound unwanted particles of a substance.

When implementing the plasma sputtering (physical vapor deposition (PVD) method of thin film deposition by sputtering that involves ejecting material from a target (source) onto a substrate (part)), a necessary condition is the presence of an additional voltage. A voltage is applied between the plasma and the substrate. Typically, the “floating potential” is about 10–20 V. Plasma sputtering is a more productive process. For example, a contaminated $h = 100$ nm layer can be removed in 500 s [128,129].

Plasma spray cleaning can be accompanied by removing the main part of the substrate material. In addition, the formation of surface defects is also possible [130].

Plasma spray cleaning can be accompanied by removing the main part of the substrate material. In addition, the formation of surface defects is also possible. Atoms or radicals chemically interact with the substrate during the plasma etching process. The first stage of plasma etching is adsorption, which is determined by the chemical composition of the substrate and temperature. Then, two ways of interaction are possible [131,132]: either adsorbed atoms and molecules interact with the surface or desorbed without chemical interaction. When volatile compounds are formed, atoms and radicals are desorbed into the gas phase and removed by pumping. Too high a temperature enhances desorption from the plasma. There is an optimum temperature when the etching process has the highest speed and slight heating of the treated surface. A combination of the above processes can give the highest cleaning efficiency.

The main parameters of surface treatment with atmospheric pressure plasma flows are the type of used inert working gas, the time of exposure to the substrate during cleaning, and the power of the plasma generator source.

These parameters affect the degree of plasma flow ionization, which determines the quality of cleaning [133].

In addition, the quality of plasma cleaning is affected by the duration of the process and the power of the plasma generator used, which implements a particular type of discharge, which must be taken into account to prevent overheating the surface of the parts during cleaning. The efficiency of plasma cleaning depends on many factors, starting with the substrate material, the duration of plasma exposure, the discharge used, the gas, the features of the physicochemical processes occurring during plasma treatment, the design features of the equipment used, and the parameters of the surrounding working environment.

The conducted analysis showed that the oxide phase can be removed effectively by one of the described plasma methods, and even more, oxide film formation can be minimized by plasma cleaning using additional ion bombardment.

4. Research of Atmospheric Plasma Sources Based on a Dielectric Barrier and Other Discharges as a Part of a Production Setup

4.1. Characteristics of Atmospheric Plasma Sources

Atmospheric plasma sources are designed to activate and clean metal and non-metal surfaces, apply thin films, air purification, surface preparation before coating deposition,

gluing, painting, etc. In addition, atmospheric plasma can be used to clean the surface of organic and biological contaminants, dust particles, and oxides.

Various plasma sources are used to clean the surface from the oxide phase and other contaminants (Table 5). Special attention is paid to high-frequency (HF) and super-high-frequency (SHF) plasma sources that are carefully considered below.

Table 5. Comparison of low- and high-pressure plasma sources.

| Name | Pressure Type | Medium | Process | Features | Notes | Reference |
|--|---------------|-------------|--|--|--|-----------|
| DC glow discharge | low | vacuum | electron bombardment (plasma cleaning by etching) | the product is located on the anode | An additional power supply is required, discharge combustion stabilization system can lead to the creation of defects, an additional power supply is required, a system for stabilizing the burning of the discharge | [134] |
| | | | ion bombardment (surface sputtering) | the product is located on the cathode ($E \approx 10^2\text{--}10^3$ eV) | | |
| High frequency discharge | low | vacuum | plasma etching | the product is located on a grounded electrode | used for cleaning metals and dielectrics | [135] |
| | | | ion etching | the product is located on the power electrode | used for cleaning metals and dielectrics | [136] |
| | | | plasma etching (reduced ion energy) | the product is located on a separate electrode | “soft” mode of plasma etching | [137] |
| Glow discharges with a hollow cathode | low | vacuum | HF-discharge (plasma cleaning, etching) | high density of plasma | high energy efficiency, low temperature | [138,139] |
| | | | magnetron etching and sputtering | uses a strong magnetic field | application of magnetron type discharge | [140] |
| Super high frequency discharge | low | vacuum | microwave plasma with high radical density for cleaning and etching | high rate of chemical reactions | electronic cyclotron mode | [141] |
| Dielectric barrier discharge (DBD) systems | high | atmospheric | plasma filamentary discharge cleaning | frequency of $10\text{--}10^4$ Hz, a continuous energy source must provide the required degree of ionization | use of high-velocity gas streams to remove cleaning products | [142] |
| Capillary barrier discharge | high | atmospheric | plasma cleaning by a filamentary discharge implemented by a device with a dielectric material with a number of small holes | the uniformity of the discharge depends on the location of the capillaries | provides a higher plasma density, the possibility of the appearance of unwanted substances on the substrate | [143] |

Table 5. Cont.

| Name | Pressure Type | Medium | Process | Features | Notes | Reference |
|--|---------------|-------------|-----------------------------|--|--|-----------|
| Corona discharge | high | atmospheric | plasma cleaning and etching | use of a needle (wire) electrode use of a planar electrode | the addition of oxygen is required for the decomposition of organic contaminants, the possibility of surface oxidation, and the decomposition of cleaning products | [144] |
| High frequency and super high frequency discharges | high | atmospheric | HF-cleaning SHF-cleaning | the conditions are realized as in the case of a glow discharge; the plasma is generated in He, N ₂ , Helium with the addition of 1–3% gas (O ₂ , N ₂ , H ₂ , or CF ₄). parameters within the arc and atmospheric pressure glow discharge | high energy efficiency, low temperature provides significant heating of the cleaned surface | [145] |

High frequency (HF) discharges can carry out surface cleaning, microwave discharges, plasma flows, and dielectric barrier discharge (DBD) systems [146–150]. These sources are of low and high pressure operating in a vacuum and at atmospheric pressure.

Plasma processes at atmospheric pressure do not require the use of expensive vacuum equipment. In addition, time is not wasted during the implementation of the technological process to create a vacuum. However, the process of plasma cleaning at atmospheric pressure also has disadvantages [151,152]: cleaning with a plasma flow requires the use of shielding gases. The process is carried out in sealed volumes using high-velocity gas flows to prevent re-contamination of the surface with cleaning products.

Atmospheric pressure plasma sources used for surface cleaning include:

- Sources of dielectric barrier discharge (DBD);
- Sources realizing pulsed direct current discharges (corona discharge);
- HF and SHF frequency sources.

4.2. Sources of Dielectric Barrier Discharge

One of the promising sources of plasma at high pressures is an electric discharge controlled by dielectric barriers, the so-called dielectric barrier discharge [153].

The design of the Dielectric Barrier Discharge (DBD) source can be implemented according to the traditional scheme and using a dielectric electrode, which has a number of small-holed capillaries.

Operating principle. DBD sources generate nonequilibrium plasma with a relatively low gas temperature. AC power sources generate the discharge power with 10–104 Hz frequencies. The DBD source consists of two plane-parallel electrodes, one of which is covered with a dielectric material (Figure 4) [154,155]. There are design schemes when both electrodes are covered with a dielectric material. An alternating voltage of 50–20,000 Hz is used when generating a discharge. The amplitude significantly exceeds the breakdown voltage. Microdischarges that occur locally are evenly distributed over the interelectrode gap. The gap between the electrodes is more than 1.5 mm. The gap size varies and depends

on the gas and its pressure. Glass, quartz, ceramics, and polymers are used as dielectric materials. Distinguish discharges by geometry, volumetric, and surface.

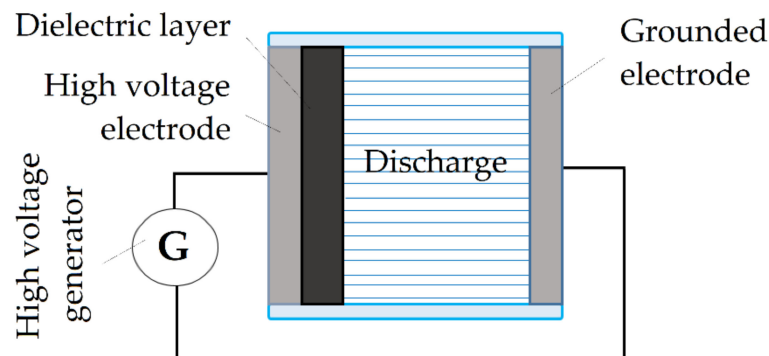


Figure 4. DBD device used for surface cleaning.

The charges are collected on the dielectric surface and discharged in microseconds during operation. The discharge exists at a certain degree of ionization. The gas filling the discharge gap causes the emission of a photon during the discharge, and the frequency and energy of the photon correspond to the type of gas [156].

Other devices for implementing the discharge have also been developed. For example, a device has been developed that implements the DBD method, characterized in that a high-resistance dielectric layer is used to cover one of the electrodes. Such a device generates a discharge called a resistive barrier, and a gallium arsenide (GaAs) semiconductor layer can be used as the dielectric layer.

The rate of purification by a device implementing DBD depends on the plasma gas composition. For example, adding a few percent of gaseous O_2 to the composition of the inert gas Ar makes it possible to intensify the process. However, a higher concentration of O_2 leads to slower removal of surface contamination or to the formation of an undesirable oxide layer. Nitrogen can also be additionally introduced into the composition of the mixture, which also contributes to a better purification process [157].

Source advantages are in the possibility of implementing DBD in technologically simple installations at atmospheric pressure, high electric field strength, soft impact on the treated surface. Disadvantages are limited length of the discharge gap, increased energy consumption.

In addition, in the practice of implementing cleaning with a dielectric barrier discharge, a device can be used in which the dielectric electrode has a number of small holes and capillaries. Such a device implements a capillary barrier discharge. Finally, a diagram of a device that implements a capillary barrier discharge is shown in Figure 5 [158].

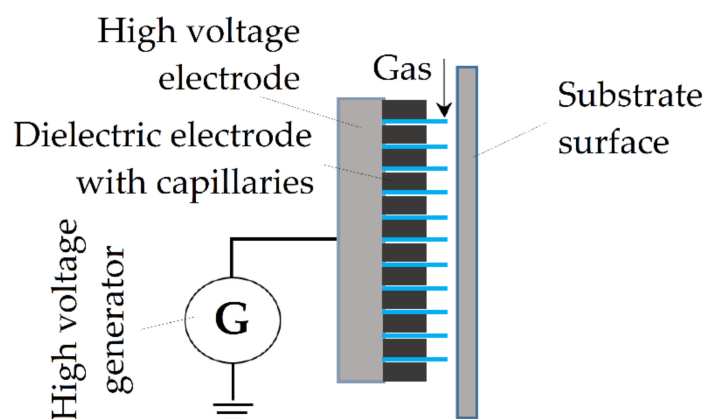


Figure 5. Capillary discharge device used for surface cleaning.

Operating principle. A discharge implemented by a DBD source ignited at atmospheric pressure in a nitrogen working gas environment or in air. As in the implementation of the above discharge, a dielectric barrier is installed between the electrodes, in which there are holes and capillaries. The temperature and density of the plasma of a capillary barrier discharge depend on the initial pressure of the gas, its chemical composition, the diameter of the hole (capillary), and the amplitude value of the current [159]. In addition, the high plasma density allows a higher cleaning power to be achieved.

In contrast to the discharge implemented by the DBD source, a capillary discharge produces stable plasma flows up to 4 cm long. The uniformity of the discharge, in turn, depends on the location of the holes in the dielectric electrode [151]. Source advantage is greater cleaning efficiency compared with traditional DBD. A flaw is in the possibility of surface damage and the deposition of undesirable substances on the substrate.

4.3. Sources of Corona Discharge

Plasma sources realizing a corona discharge operate in an electric field with high intensity, at high air pressure. Ionization processes during discharge generation occur only near the corona electrode. The diagram of the device is shown in Figure 4.

Operating principle. Using a corona discharge for cleaning the surface is possible using non-uniform fields that occur at electrodes with large surface curvature. Such an independent discharge is typical for electrodes in point, thin wires. Near such cathodes, a corona-shaped glow appears, and the field strength has higher values. The flow of a corona discharge is observed if an electron arises during the random ionization of a molecule (neutral). It accelerates in the electric field, acquiring energy enough to ionize another molecule. As a result of the process, a new negative electron and a positively charged ion are formed. Thus, a stream of charged particles is formed that then passes into an avalanche. The characteristics of a corona discharge depend on the type of corona (negative or positive) and the pulse applied to the corona electrode [160,161]. The scheme of the device that implements the corona discharge is shown in Figure 6.

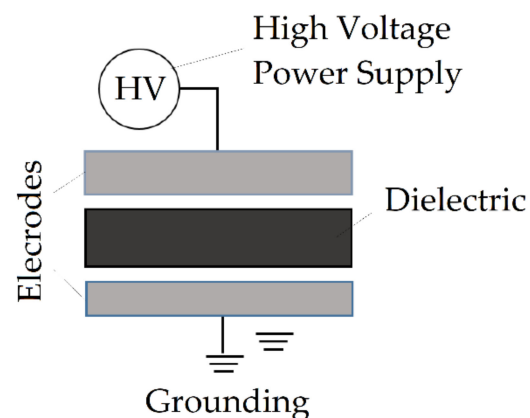


Figure 6. Corona devices used for surface cleaning.

Corona discharge device configurations use needle electrodes (thin wire) or planar electrodes. In this case, the energy is concentrated on the needle electrode, and the flat one is grounded. The addition of oxygen is necessary for the decomposition of organic pollutants. Voltage during processing is applied to the upper electrode. The dielectric in the system is located between two electrodes and air gaps. The bottom electrode is grounded. The gradually increasing voltage ionizes the air between the two electrodes and creates a corona discharge.

The main source advantage is in the ability to initiate a chemical reaction on the surface to be cleaned. Flaws are significant weakening of the plasma effect during processing, oxidation of the substrate surface due to ozone release, and the need for sophisticated ozone neutralization equipment.

4.4. High Frequency and Super High Frequency Discharges

For excitation in sources of High Frequency (HF) and Super High Frequency (SHF) (microwave) discharges, two electrodes must be in direct contact with the plasma. The direct current glow discharge is ignited and maintained, which is necessary to implement the cleaning process. However, such conditions can lead to disruption of the discharge due to the formation of a non-conductive film on the electrodes. The diagram of the device is shown in Figure 7 [162,163].

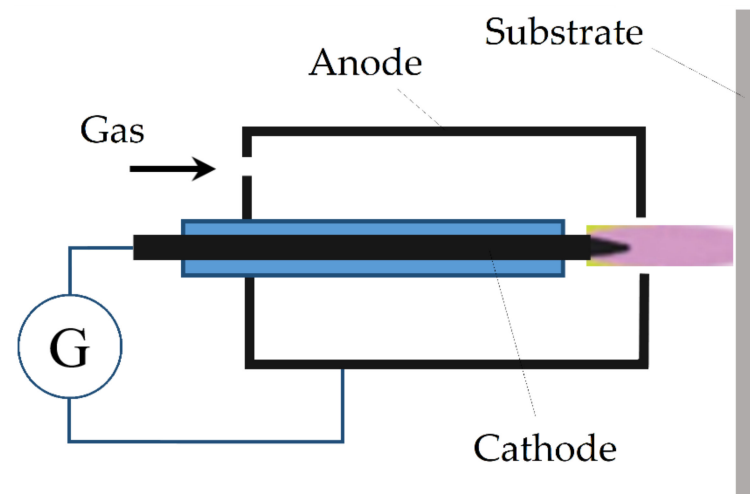


Figure 7. Plasma source for surface cleaning.

Atmospheric glow discharge is generated using a high-frequency discharge and microwave (microwave) at high pressure. Plasma is generated in He, N₂, air, and He with the addition of 1–3% molecular gas such as O₂, N₂, H₂, or CF₄, providing sufficient concentration of the plasma stream to clean the surface material effectively.

The atmospheric pressure plasma source is a device with an internal electrode and a grounded external electrode. The plasma gas flows between the electrodes at high speed and exits the nozzle. The plasma jet propagates from the anode (the anode is grounded). Plasma source operating modes: voltage of several hundred volts, power~1 kW. Surface treatment can be realized in HF and microwave modes. Plasma is generated in the resonant chamber and enters the processing zone through the opening-nozzle in the chamber [129,157]. The parameters of the plasma realizing the microwave discharge are close to the parameters of the arc and glow discharge of atmospheric pressure.

Device advantages are in the possibility of modifying the surface to be cleaned; the ability to control chemically active substances to improve the quality of cleaning.

Flaws are in limited areas of impact of HF and SHF discharge; there is significant heating of the substrate in the process of exposure to the source, and possible overheating of the surface. A plasma source based on atmospheric plasma based on a dielectric barrier discharge is most suitable for use as a source of plasma surface cleaning.

5. Conclusions

Today, the introduction of additive technologies, particularly LPBF in production, is hampered by the lack of scientifically based recommendations on the choice of process parameters for newly introduced metal-based materials and alloys. It is related to the lack of systematic studies of the LPBF, the influence of its factors on the quality of grown products, the formation of defects related to the presence of the oxide phase in the structure of the solids, and the lack of critical engineering solutions to minimize these types of structural defects and surface roughness. The analysis of oxide phase formation shows that the formation of structural and surface defects such as cracks, pores, oxide phases, etc., is

determined by many process factors and related to the LPBF specifics depending on the chosen modes, material, and powder properties (reflectivity, sphericity, etc.).

Surface plasma cleaning methods demonstrate their ability to remove the oxide phase in metal products that can be used in laser powder bed fusion as a part of the unit. This provides conditions for reliable product growing that can be even more durable in extreme conditions by removing the oxide phase, smoothing the surface, and recrystallization by heat treatment (decrease in grain size). Systematization and comparative analysis of the existed plasma-based methods provided by different types of plasma sources for physical surface cleaning have shown that the plasma processing using additional ion bombardment by a plasma source based on an electric discharge with a dielectric barrier can be preferable to minimize the oxide phase and other structural and surface defects after LPBF.

Using a newly developed plasma source as a part of the LPBF unit can significantly reduce the labor intensity of production engineering products with the specific requirements to their physical and mechanical properties and surface quality and, in prospect, enlarge their exploitation ability and service life for working in cyclic loads.

Developing the LPBF production setup equipped with an atmospheric plasma source based on a dielectric barrier discharge could contribute to creating a new type of hybrid equipment for transition to the sixth technological paradigm associated with Kondratieff's waves.

6. Patents

Grigoriev Sergey Nikolaevich; Metel Alexander Sergeevich; Volosova Marina Alexandrovna; Melnik Yury Andreevich; Mustafaev Enver Serverovich. Device for processing dielectric products with fast atoms; #RU2752877C1, 2020-12-11.

Author Contributions: Conceptualization, S.N.G. and M.A.V.; methodology, S.V.F. and A.S.M.; software, S.V.F. and N.A.S.; validation, A.S.M. and S.R.S.; formal analysis, A.S.M. and A.A.O.; investigation, S.V.F.; resources, N.A.S.; data curation, S.R.S.; writing—original draft preparation, S.R.S. and N.A.S.; writing—review and editing, A.A.O. and M.A.V.; visualization, S.R.S. and N.A.S.; supervision, S.N.G.; project administration, S.N.G. and M.A.V.; funding acquisition, A.S.M. All authors have read and agreed to the published version of the manuscript.

Funding: This research was funded by the Russian Science Foundation, grant number No. 20-19-00620.

Institutional Review Board Statement: Not applicable.

Informed Consent Statement: Not applicable.

Data Availability Statement: Data are available in a publicly accessible repository.

Acknowledgments: The research was conducted at the Department of High-Efficiency Processing Technologies of MSTU Stankin.

Conflicts of Interest: The authors declare no conflict of interest.

References

1. Aversa, A.; Marchese, G.; Saboori, A.; Bassini, E.; Manfredi, D.; Biamino, S.; Ugues, D.; Fino, P.; Lombardi, M. New Aluminum Alloys Specifically Designed for Laser Powder Bed Fusion: A Review. *Materials* **2019**, *12*, 1007. [[CrossRef](#)] [[PubMed](#)]
2. Denti, L. Additive Manufactured A357.0 Samples Using the Laser Powder Bed Fusion Technique: Shear and Tensile Performance. *Metals* **2018**, *8*, 670. [[CrossRef](#)]
3. Sova, A.; Grigoriev, S.; Okunkova, A.; Smurov, I. Potential of cold gas dynamic spray as additive manufacturing technology. *Int. J. Adv. Manuf. Technol.* **2013**, *69*, 2269–2278. [[CrossRef](#)]
4. Sova, A.; Grigoriev, S.; Okunkova, A.; Bertrand, P.; Smurov, I. Cold spraying: From process fundamentals towards advanced applications. *Surf. Coat. Technol.* **2015**, *268*, 77–84.
5. Notenboom, G.; Maerten, O. Additive mass manufacturing of composite ceramic, metal and glass microparts and multilayers from nanosized particles, using inkjet and laser technology (Acerlink). In *5th European Conference on Advanced Materials and Processes and Applications (EUROMAT 97), Proceedings of the 5th European Conference on Advanced Materials and Processes and Applications: Materials, Functionality & Design, Maastricht, The Netherlands, 21–23 April 1997*; Sarton, L.A.J., Zeedijk, H.B., Eds.; Netherlands Soc Materials Science: Zwijndrecht, The Netherlands, 1997; Volume 3, p. 55.

6. Kumar, M.S. Rapid Prototyping-An overview of the present state-of-the-art. In Proceedings of the 13th National Convention of Mechanical Engineers, Modern Trends in Manufacturing Technology, Maastricht, The Netherlands, 6–8 November 1997; Chaturvedi, P., Tewari, N.K., Yadav, G.S., Rao, P.V., Eds.; Concept Publ Co.: New Delhi, India, 1998; pp. 123–130.
7. Aleshin, N.P.; Grigor'ev, M.V.; Shchipakov, N.A.; Prilutskii, M.A.; Murashov, V.V. Applying nondestructive testing to quality control of additive manufactured parts. *Russ. J. Nondestruct. Test.* **2016**, *52*, 600–609. [[CrossRef](#)]
8. Metel, A.S.; Grigoriev, S.N.; Tarasova, T.V.; Melnik, Y.A.; Volosova, M.A.; Okunkova, A.A.; Podrabinnik, P.A.; Mustafaev, E.S. Surface Quality of Metal Parts Produced by Laser Powder Bed Fusion: Ion Polishing in Gas-Discharge Plasma Proposal. *Technologies* **2021**, *9*, 27. [[CrossRef](#)]
9. Liu, D.; Lee, B.; Babkin, A.; Chang, Y. Research Progress of Arc Additive Manufacture Technology. *Materials* **2021**, *14*, 1415. [[CrossRef](#)]
10. Grigor'yants, A.G.; Shiganov, I.N. Development of Domestic Equipment for Laser Additive Technologies by Melting Metallic Powders. *Russ. Metall.* **2020**, *6*, 649–653. [[CrossRef](#)]
11. Ivanov, A.D.; Minaev, V.L.; Vishnyakov, G.N. A Shearograph for Nondestructive Testing of Products Obtained by Additive Technologies. *Instrum. Exp. Tech.* **2019**, *62*, 871–875. [[CrossRef](#)]
12. Kurbatov, A.S.; Orekhov, A.A.; Rabinskiy, L.N.; Tushavina, O.V.; Kuznetsova, E.L. Research of The Problem of Loss of Stability of Cylindrical Thin-Walled Structures Under Intense Local Temperature Exposure. *Period. Tche Quim.* **2020**, *17*, 884–891.
13. Khmyrov, R.S.; Grigoriev, S.N.; Okunkova, A.A.; Gusarov, A.V. On the possibility of selective laser melting of quartz glass. *Phys. Procedia* **2014**, *56*, 345–356. [[CrossRef](#)]
14. Khmyrov, R.S.; Protasov, C.E.; Grigoriev, S.N.; Gusarov, A.V. Crack-free selective laser melting of silica glass: Single beads and monolayers on the substrate of the same material. *Int. J. Adv. Manuf. Technol.* **2016**, *85*, 1461–1469. [[CrossRef](#)]
15. Grigoriev, S.; Peretyagin, P.; Smirnov, A.; Solis, W.; Diaz, L.A.; Fernandez, A.; Torrecillas, R. Effect of graphene addition on the mechanical and electrical properties of Al₂O₃-SiCw ceramics. *J. Eur. Ceram. Soc.* **2017**, *37*, 2473–2479. [[CrossRef](#)]
16. Sova, A.; Grigoriev, S.; Okunkova, A.; Smurov, I. Cold spray deposition of 316L stainless steel coatings on aluminium surface with following laser post-treatment. *Surf. Coat. Technol.* **2013**, *235*, 283–289. [[CrossRef](#)]
17. Klingaa, C.G.; Mohanty, S.; Hjermitslev, A.B.; Haahr-Lillevang, L.; Hattel, J.H. Towards a digital twin of laser powder bed fusion with a focus on gas flow variables. *J. Manuf. Process.* **2021**, *65*, 312–327. [[CrossRef](#)]
18. Kozior, T.; Bochnia, J. The Influence of Printing Orientation on Surface Texture Parameters in Powder Bed Fusion Technology with 316L Steel. *Micromachines* **2020**, *11*, 639. [[CrossRef](#)]
19. Asnafi, N. Application of Laser-Based Powder Bed Fusion for Direct Metal Tooling. *Metals* **2021**, *11*, 458. [[CrossRef](#)]
20. Grigor'ev, S.N.; Kozochkin, M.P.; Fedorov, S.V.; Porvatov, A.N.; Okun'kova, A.A. Study of Electroerosion Processing by Vibroacoustic Diagnostic Methods. *Meas. Tech.* **2015**, *58*, 878–884. [[CrossRef](#)]
21. Vila, C.; Siller, H.R.; Rodriguez, C.A.; Bruscas, G.M.; Serrano, J. Economical and technological study of surface grinding versus face milling in hardened AISI D3 steel machining operations. *Int. J. Prod. Econ.* **2012**, *138*, 273–283. [[CrossRef](#)]
22. Bekem, A.; Ozbay, B.; Bulduk, M.E. Effect of dendritic copper powder addition to polyamide 12 in selective laser sintering. *J. Fac. Eng. Archit. Gazi Univ.* **2021**, *36*, 421–431.
23. Qin, Y.L.; Sun, B.H.; Zhang, H.; Ni, D.R.; Xiao, B.L.; Ma, Z.Y. Development of Selective Laser Melted Aluminum Alloys and Aluminum Matrix Composites in Aerospace Field. *Chin. J. Lasers-Zhongguo Jiguang* **2021**, *48*, 1402002.
24. Wang, H.; Chen, J.Q.; Luo, H.L.; Wang, D.; Song, C.H.; Yao, X.Y.; Chen, P.; Yan, M. Bimetal printing of high entropy alloy/metallic glass by laser powder bed fusion additive manufacturing. *Intermetallics* **2022**, *141*, 107430. [[CrossRef](#)]
25. Sova, A.; Okunkova, A.; Grigoriev, S.; Smurov, I. Velocity of the Particles Accelerated by a Cold Spray Micronozzle: Experimental Measurements and Numerical Simulation. *J. Therm. Spray Technol.* **2012**, *22*, 75–80. [[CrossRef](#)]
26. Santecchia, E.; Spigarelli, S.; Cabibbo, M. Material Reuse in Laser Powder Bed Fusion: Side Effects of the Laser—Metal Powder Interaction. *Metals* **2020**, *10*, 341. [[CrossRef](#)]
27. Grigoriev, S.N.; Kozochkin, M.P.; Porvatov, A.N.; Volosova, M.A.; Okunkova, A.A. Electrical discharge machining of ceramic nanocomposites: Sublimation phenomena and adaptive control. *Heliyon* **2019**, *5*, e02629. [[CrossRef](#)] [[PubMed](#)]
28. Khorasani, M.; Ghasemi, A.; Rolfe, B.; Gibson, I. Additive manufacturing a powerful tool for the aerospace industry. *Rapid Prototyp. J.* **2022**, *28*, 87–100. [[CrossRef](#)]
29. Mindt, H.W.; Desmaison, O.; Megahed, M.; Peralta, A.; Neumann, J. Modeling of Powder Bed Manufacturing Defects. *J. Mater. Eng. Perform.* **2018**, *27*, 32–43. [[CrossRef](#)]
30. Metel, A.S.; Grigoriev, S.N.; Tarasova, T.V.; Filatova, A.A.; Sundukov, S.K.; Volosova, M.A.; Okunkova, A.A.; Melnik, Y.A.; Podrabinnik, P.A. Influence of Postprocessing on Wear Resistance of Aerospace Steel Parts Produced by Laser Powder Bed Fusion. *Technologies* **2020**, *8*, 73. [[CrossRef](#)]
31. Mahmood, M.A.; Ur Rehman, A.; Pitir, F.; Salamci, M.U.; Mihailescu, I.N. Laser Melting Deposition Additive Manufacturing of Ti6Al4V Biomedical Alloy: Mesoscopic In-Situ Flow Field Mapping via Computational Fluid Dynamics and Analytical Modelling with Empirical Testing. *Materials* **2021**, *14*, 7749. [[CrossRef](#)]
32. Dostovalov, A.V.; Korolkov, V.P.; Babin, S.A. Formation of thermochemical laser-induced periodic surface structures on Ti films by a femtosecond IR Gaussian beam: Regimes, limiting factors, and optical properties. *Appl. Phys. B-Lasers Opt.* **2017**, *123*, 30. [[CrossRef](#)]

33. Gusarov, A.V.; Grigoriev, S.N.; Volosova, M.A.; Melnik, Y.A.; Laskin, A.; Kotoban, D.V.; Okunkova, A.A. On productivity of laser additive manufacturing. *J. Mater. Process. Technol.* **2018**, *261*, 213–232. [[CrossRef](#)]
34. Yadroitsev, I.; Bertrand, P.H.; Antonenkova, G.; Grigoriev, S.; Smurov, I. Use of track/layer morphology to develop functional parts by selective laser melting. *J. Laser Appl.* **2013**, *25*, 052003. [[CrossRef](#)]
35. Kotoban, D.; Grigoriev, S.; Okunkova, A.; Sova, A. Influence of a shape of single track on deposition efficiency of 316L stainless steel powder in cold spray. *Surf. Coat. Technol.* **2017**, *309*, 951–958. [[CrossRef](#)]
36. Doubenskaia, M.; Pavlov, M.; Grigoriev, S.; Tikhonova, E.; Smurov, I. Comprehensive Optical Monitoring of Selective Laser Melting. *J. Laser Micro Nanoeng.* **2012**, *7*, 236–243. [[CrossRef](#)]
37. Glaziev, S.Y. The discovery of regularities of change of technological orders in the central economics and mathematics institute of the soviet academy of sciences. *Econ. Math. Methods* **2018**, *54*, 17–30. [[CrossRef](#)]
38. Korotayev, A.V.; Tsirel, S.V. A spectral analysis of world GDP dynamics: Kondratiev waves, Kuznets swings, Juglar and Kitchin cycles in global economic development, and the 2008–2009 economic crisis. *Struct. Dyn.* **2010**, *4*, 3–57. [[CrossRef](#)]
39. Perez, C. Technological revolutions and techno-economic paradigms. *Camb. J. Econ.* **2010**, *34*, 185–202. [[CrossRef](#)]
40. Wonglimpiyarat, J. Towards the sixth Kondratieff cycle of nano revolution. *Int. J. Nanotechnol. Mol. Comput.* **2011**, *3*, 87–100. [[CrossRef](#)]
41. Smurov, I.; Doubenskaia, M.; Grigoriev, S.; Nazarov, A. Optical Monitoring in Laser Cladding of Ti6Al4V. *J. Spray Technol.* **2012**, *21*, 1357–1362. [[CrossRef](#)]
42. Scotti, F.M.; Teixeira, F.R.; da Silva, L.J.; de Araujo, D.B.; Reis, R.P.; Scotti, A. Thermal management in WAAM through the CMT Advanced process and an active cooling technique. *J. Manuf. Process.* **2020**, *57*, 23–35. [[CrossRef](#)]
43. Duman, B.; Ozsoy, K. A deep learning-based approach for defect detection in powder bed fusion additive manufacturing using transfer learning. *J. Fac. Eng. Archit. Gazi Univ.* **2022**, *37*, 361–375.
44. Sing, S.L.; Yeong, W.Y.; Wiria, F.E.; Tay, B.Y.; Zhao, Z.Q.; Zhao, L.; Tian, Z.L.; Yang, S.F. Direct selective laser sintering and melting of ceramics: A review. *Rapid Prototyp. J.* **2017**, *23*, 611–623. [[CrossRef](#)]
45. Deirmina, F.; Davies, P.A.; Casati, R. Effects of Powder Atomization Route and Post-Processing Thermal Treatments on the Mechanical Properties and Fatigue Resistance of Additively Manufactured 18Ni300 Maraging Steel. *Adv. Eng. Mater.* **2021**, *24*, 2101011. [[CrossRef](#)]
46. Yan, J.; Zhou, Y.; Gu, R.; Zhang, X.; Quach, W.-M.; Yan, M. A Comprehensive Study of Steel Powders (316L, H13, P20 and 18Ni300) for Their Selective Laser Melting Additive Manufacturing. *Metals* **2019**, *9*, 86. [[CrossRef](#)]
47. Metel, A.; Tarasova, T.; Gutsaliuk, E.; Khmyrov, R.; Egorov, S.; Grigoriev, S. Possibilities of Additive Technologies for the Manufacturing of Tooling from Corrosion-Resistant Steels in Order to Protect Parts Surfaces from Thermochemical Treatment. *Metals* **2021**, *11*, 1551. [[CrossRef](#)]
48. Fomin, V.M.; Golyshv, A.A.; Malikov, A.G.; Orshich, A.M.; Filippov, A.A. Creation of A Functionally Gradient Material by the Selective Laser Melting Method. *J. Appl. Mech. Tech. Phys.* **2020**, *61*, 878–887. [[CrossRef](#)]
49. Akopyan, T.K.; Letyagin, N.V.; Avxentieva, N.N. High-tech alloys based on Al-Ca-La(-Mn) eutectic system for casting, metal forming and selective laser melting. *Non-Ferr. Met.* **2020**, *1*, 52–59. [[CrossRef](#)]
50. Mazeeva, A.K.; Staritsyn, M.V.; Bobyr, V.V.; Manninen, S.A.; Kuznetsov, P.A.; Klimov, V.N. Magnetic properties of Fe-Ni permalloy produced by selective laser melting. *J. Alloy. Compd.* **2020**, *814*, 152315. [[CrossRef](#)]
51. Samodurova, M.; Logachev, I.; Shaburova, N.; Samoilova, O.; Radionova, L.; Zakirov, R.; Pashkeev, K.; Myasoedov, V.; Trofimov, E. A Study of the Structural Characteristics of Titanium Alloy Products Manufactured Using Additive Technologies by Combining the Selective Laser Melting and Direct Metal Deposition Methods. *Materials* **2019**, *12*, 3269. [[CrossRef](#)]
52. Okunkova, A.; Peretyagin, P.; Vladimirov, Y.; Volosova, M.; Torrecillas, R.; Fedorov, S.V. Laser-beam modulation to improve efficiency of selecting laser melting for metal powders. In Proceedings of the Conference on Laser Sources and Applications II, Laser Sources and Applications II, Laser Sources and Applications II, Brussels, Belgium, 14–17 April 2014; Mackenzie, J.I., Jelinkova, H., Taira, T., Ahmed, M.A., Eds.; SPIE-Int Soc Optical Engineering: Bellingham, WA, USA, 2014; Volume 9135, p. 913524.
53. Gusarov, A.V.; Okunkova, A.A.; Peretyagin, P.Y.; Zhirnov, I.V.; Podrabinnik, P.A. Means of Optical Diagnostics of Selective Laser Melting with Non-Gaussian Beams. *Meas. Tech.* **2015**, *58*, 872–877. [[CrossRef](#)]
54. Gu, R.N.; Wong, K.S.; Yan, M. Laser additive manufacturing of typical highly reflective materials-gold, silver and copper. *Sci. Sin. Phys. Mech. Astron.* **2020**, *50*, 034204.
55. Klotz, U.E.; Tiberto, D.; Held, F. Optimization of 18-karat yellow gold alloys for the additive manufacturing of jewelry and watch parts. *Gold Bull.* **2017**, *50*, 111–121. [[CrossRef](#)]
56. Chauveau, D. Review of NDT and process monitoring techniques usable to produce high-quality parts by welding or additive manufacturing. *Weld. World* **2018**, *62*, 1097–1118. [[CrossRef](#)]
57. Shi, Y.S.; Zhang, J.L.; Wen, S.F.; Song, B.; Yan, C.Z.; Wei, Q.S.; Wu, J.M.; Yin, Y.J.; Zhou, J.X.; Chen, R.; et al. Additive manufacturing and foundry innovation. *China Foundry* **2021**, *18*, 286–295. [[CrossRef](#)]
58. Yang, L.; Tang, S.Y.; Fan, Z.T.; Jiang, W.M.; Liu, X.W. Rapid casting technology based on selective laser sintering. *China Foundry* **2021**, *18*, 296–306. [[CrossRef](#)]
59. Abdul Rani, A.M.; Fua-Nizan, R.; Din, M.Y. Manufacturing methods for medical artificial prostheses—A review. *Malays. J. Fundam. Appl. Sci.* **2017**, *13*, 464–469.

60. Li, Y.; Li, D.C.; Lu, B.H.; Gao, D.J.; Zhou, J. Current status of additive manufacturing for tissue engineering scaffold. *Rapid Prototyp. J.* **2015**, *21*, 747–762. [[CrossRef](#)]
61. Ojo, O.O.; Taban, E. Defects and post-manufacturing processes of additively manufactured steels: A Review (Part 2). *Mater. Test.* **2020**, *62*, 835–848.
62. Filatova, A.; Tarasova, T.; Peretyagin, P. Developing processes for manufacturing metal aviation technology components using powder bed fusion methods. *MATEC Web Conf.* **2019**, *298*, 00116. [[CrossRef](#)]
63. Cortina, M.; Arrizubieta, J.I.; Calleja, A.; Ukar, E.; Alberdi, A. Case Study to Illustrate the Potential of Conformal Cooling Channels for Hot Stamping Dies Manufactured Using Hybrid Process of Laser Metal Deposition (LMD) and Milling. *Metals* **2018**, *8*, 102. [[CrossRef](#)]
64. Zhao, Y.; Li, F.; Chen, S.; Lu, Z.Y. Unit block-based process planning strategy of WAAM for complex shell-shaped component. *Int. J. Adv. Manuf. Technol.* **2019**, *104*, 3915–3927. [[CrossRef](#)]
65. Han, P. Additive Design and Manufacturing of Jet Engine Parts. *Engineering* **2017**, *3*, 648–652. [[CrossRef](#)]
66. Ghaffari, M.; Nemani, A.V.; Rafieezad, M.; Nasiri, A. Effect of Solidification Defects and HAZ Softening on the Anisotropic Mechanical Properties of a Wire Arc Additive-Manufactured Low-Carbon Low-Alloy Steel Part. *JOM* **2019**, *71*, 4215–4224. [[CrossRef](#)]
67. Sun, X.F.; Song, W.; Liang, J.J.; Li, J.G.; Zhou, Y.Z. Research and Development in Materials and Processes of Superalloy Fabricated by Laser Additive Manufacturing. *Acta Metall. Sin.* **2021**, *57*, 1471–1483.
68. Magerramova, L.; Isakov, V.; Shcherbinina, L.; Gukasyan, S.; Petrov, M.; Povalyukhin, D.; Volosevich, D.; Klimova-Korsmik, O. Design, Simulation and Optimization of an Additive Laser-Based Manufacturing Process for Gearbox Housing with Reduced Weight Made from AlSi10Mg Alloy. *Metals* **2022**, *12*, 67. [[CrossRef](#)]
69. Brailovski, V.; Kalinicheva, V.; Letenneur, M.; Lukashevich, K.; Sheremetyev, V.; Prokoshkin, S. Control of Density and Grain Structure of a Laser Powder Bed-Fused Superelastic Ti-18Zr-14Nb Alloy: Simulation-Driven Process Mapping. *Metals* **2020**, *10*, 1697. [[CrossRef](#)]
70. Ahsan, F.; Razmi, J.; Ladani, L. Process Parameter Optimization in Metal Laser-Based Powder Bed Fusion Using Image Processing and Statistical Analyses. *Metals* **2022**, *12*, 87. [[CrossRef](#)]
71. Gurin, V.D.; Kotoban, D.V.; Podrabinnik, P.A.; Zhirnov, I.V.; Peretyagin, P.Y.; Okunkova, A.A. Modeling of 3D technological fields and research of principal perspectives and limits in productivity improvement of selective laser melting. *Mech. Ind.* **2016**, *17*, 714. [[CrossRef](#)]
72. Zhirnov, I.V.; Podrabinnik, P.A.; Okunkova, A.A.; Gusarov, A.V. Laser beam profiling: Experimental study of its influence on single-track formation by selective laser melting. *Mech. Ind.* **2015**, *16*, 709. [[CrossRef](#)]
73. Yan, Q.; Song, B.; Shi, Y.S. Comparative study of performance comparison of AlSi10Mg alloy prepared by selective laser melting and casting. *J. Mater. Sci. Technol.* **2020**, *41*, 199–208. [[CrossRef](#)]
74. Albu, M.; Panzirsch, B.; Schröttner, H.; Mitsche, S.; Reichmann, K.; Poletti, M.C.; Kothleitner, G. High-Resolution Microstructure Characterization of Additively Manufactured X5CrNiCuNb17-4 Maraging Steel during Ex and In Situ Thermal Treatment. *Materials* **2021**, *14*, 7784. [[CrossRef](#)] [[PubMed](#)]
75. Tian, Z.; Zhang, C.; Wang, D.; Liu, W.; Fang, X.; Wellmann, D.; Zhao, Y.; Tian, Y. A Review on Laser Powder Bed Fusion of Inconel 625 Nickel-Based Alloy. *Appl. Sci.* **2020**, *10*, 81. [[CrossRef](#)]
76. Sotov, A.V.; Agapovichev, A.V.; Smelov, V.G.; Kokareva, V.V.; Zenina, M.V. Investigation of the Ni-Co-Cr alloy microstructure for the manufacturing of combustion chamber GTE by selective laser melting. *Int. J. Adv. Manuf. Technol.* **2019**, *101*, 3047–3053. [[CrossRef](#)]
77. Zegzulka, J.; Gelnar, D.; Jezerska, L. Characterization and fowability methods for metal powders. *Sci. Rep.* **2020**, *10*, 21004. [[CrossRef](#)]
78. Wang, L.; Li, E.L.; Shen, H.; Zou, R.P.; Yu, A.B.; Zhou, Z.Y. Adhesion effects on spreading of metal powders in selective laser melting. *Powder Technol.* **2020**, *363*, 602–610. [[CrossRef](#)]
79. Zakharov, O.V.; Brzhozovskii, B.M. Accuracy of centering during measurement by roundness gauges. *Meas. Tech.* **2006**, *49*, 1094–1097. [[CrossRef](#)]
80. Rezhnikov, A.F.; Kochetkov, A.V.; Zakharov, O.V. Mathematical models for estimating the degree of influence of major factors on performance and accuracy of coordinate measuring machines. *MATEC Web Conf.* **2017**, *129*, 01054. [[CrossRef](#)]
81. Zakharov, O.V.; Balaev, A.F.; Kochetkov, A.V. Modeling Optimal Path of Touch Sensor of Coordinate Measuring Machine Based on Traveling Salesman Problem Solution. *Procedia Eng.* **2017**, *206*, 1458–1463. [[CrossRef](#)]
82. Grigoriev, S.N.; Metel, A.S.; Tarasova, T.V.; Filatova, A.A.; Sundukov, S.K.; Volosova, M.A.; Okunkova, A.A.; Melnik, Y.A.; Podrabinnik, P.A. Effect of Cavitation Erosion Wear, Vibration Tumbling, and Heat Treatment on Additively Manufactured Surface Quality and Properties. *Metals* **2020**, *10*, 1540. [[CrossRef](#)]
83. Lou, X.Y.; Andresen, P.L.; Rebak, R.B. Oxide inclusions in laser additive manufactured stainless steel and their effects on impact toughness and stress corrosion cracking behavior. *J. Nucl. Mater.* **2018**, *499*, 182–190. [[CrossRef](#)]
84. Zai, L.; Zhang, C.; Wang, Y.; Guo, W.; Wellmann, D.; Tong, X.; Tian, Y. Laser Powder Bed Fusion of Precipitation-Hardened Martensitic Stainless Steels: A Review. *Metals* **2020**, *10*, 255. [[CrossRef](#)]
85. Metel, A.S.; Stebulyanin, M.M.; Fedorov, S.V.; Okunkova, A.A. Power Density Distribution for Laser Additive Manufacturing (SLM): Potential, Fundamentals and Advanced Applications. *Technologies* **2019**, *7*, 5. [[CrossRef](#)]

86. Cheng, B.; Shrestha, S.; Chou, K. Stress and deformation evaluations of scanning strategy effect in selective laser melting. *Addit. Manuf.* **2016**, *12B*, 240–251.
87. Aota, L.S.; Bajaj, P.; Zilnyk, K.D.; Ponge, D.; Sandim, H.R.Z. The origin of abnormal grain growth upon thermomechanical processing of laser powder-bed fusion alloys. *Materialia* **2021**, *20*, 101243. [[CrossRef](#)]
88. Gong, H.; Nadimpalli, V.K.; Rafi, K.; Starr, T.; Stucker, B. Micro-CT Evaluation of Defects in Ti-6Al-4V Parts Fabricated by Metal Additive Manufacturing. *Technologies* **2019**, *7*, 44. [[CrossRef](#)]
89. Zhang, P.; He, A.N.; Liu, F.; Zhang, K.; Jiang, J.; Zhang, D.Z. Evaluation of Low Cycle Fatigue Performance of Selective Laser Melted Titanium Alloy Ti-6Al-4V. *Metals* **2019**, *9*, 1041. [[CrossRef](#)]
90. Loginova, I.S.; Bykovskiy, D.P.; Solonin, A.N.; Prosviryakov, A.S.; Cheverikin, V.V.; Pozdniakov, A.V.; Petrovskiy, V.N. Peculiarities of the Microstructure and Properties of Parts Produced by the Direct Laser Deposition of 316L Steel Powder. *Russ. J. Non-Ferr. Met.* **2019**, *60*, 87–94. [[CrossRef](#)]
91. Pelevin, I.A.; Ozherelkov, D.Y.; Chernyshikhin, S.V.; Nalivaiko, A.Y.; Gromov, A.A.; Chzhan, V.B.; Terekhin, E.A.; Tereshina, I.S. Selective laser melting of Nd-Fe-B: Single track study. *Mater. Lett.* **2022**, *315*, 131947. [[CrossRef](#)]
92. Tan, J.H.; Wong, W.L.E.; Dalgarno, K.W. An overview of powder granulometry on feedstock and part performance in the selective laser melting process. *Addit. Manuf.* **2017**, *18*, 228–255. [[CrossRef](#)]
93. Zhang, X.B.; Cheng, B.; Tuffile, C. Simulation study of the spatter removal process and optimization design of gas flow system in laser powder bed fusion. *Addit. Manuf.* **2020**, *32*, 101049. [[CrossRef](#)]
94. Vilanova, M.; Escibano-García, R.; Guraya, T.; San Sebastian, M. Optimizing Laser Powder Bed Fusion Parameters for IN-738LC by Response Surface Method. *Materials* **2020**, *13*, 4879. [[CrossRef](#)] [[PubMed](#)]
95. Ogawahara, M.; Sasaki, S. Effects of Defects and Inclusions on the Fatigue Properties of Inconel 718 Fabricated by Laser Powder Bed Fusion Followed by HIP. *Mater. Trans.* **2021**, *62*, 631–635. [[CrossRef](#)]
96. Aliprandi, P.; Giudice, F.; Guglielmino, E.; Sili, A. Tensile and Creep Properties Improvement of Ti-6Al-4V Alloy Specimens Produced by Electron Beam Powder Bed Fusion Additive Manufacturing. *Metals* **2019**, *9*, 1207. [[CrossRef](#)]
97. Fang, M.H.; Hu, F.G.; Han, Y.F.; Le, J.W.; Xi, J.J.; Song, J.W.; Ke, L.D.; Xiao, M.L.; Lu, W.J. Controllable mechanical anisotropy of selective laser melted Ti6Al4V: A new perspective into the effect of grain orientations and primary grain structure. *Mater. Sci. Eng. A-Struct. Mater. Prop. Microstruct. Process.* **2021**, *827*, 142031. [[CrossRef](#)]
98. Liu, J.; Liu, J.; Li, Y.; Zhang, R.; Zeng, Z.; Zhu, Y.; Zhang, K.; Huang, A. Effects of Post Heat Treatments on Microstructures and Mechanical Properties of Selective Laser Melted Ti6Al4V Alloy. *Metals* **2021**, *11*, 1593. [[CrossRef](#)]
99. Wang, C.; Yi, J.Z.; Qin, L.Y.; Wang, W.D.; Wang, X.M.; Yang, G. Effects of double annealing on microstructure and mechanical properties of laser melting deposition TA15 titanium alloy. *Mater. Res. Express* **2019**, *6*, 116526. [[CrossRef](#)]
100. Lin, D.Y.; Xu, L.Y.; Li, X.J.; Jing, H.Y.; Qin, G.; Pang, H.N.; Minami, F. A Si-containing FeCoCrNi high-entropy alloy with high strength and ductility synthesized in situ via selective laser melting. *Addit. Manuf.* **2020**, *35*, 101340. [[CrossRef](#)]
101. Miao, X.; Liu, X.; Lu, P.; Han, J.; Duan, W.; Wu, M. Influence of Scanning Strategy on the Performances of GO-Reinforced Ti6Al4V Nanocomposites Manufactured by SLM. *Metals* **2020**, *10*, 1379. [[CrossRef](#)]
102. Vrancken, B.; Ganeriwala, R.K.; Matthews, M.J. Analysis of laser-induced microcracking in tungsten under additive manufacturing conditions: Experiment and simulation. *Acta Mater.* **2020**, *194*, 464–472. [[CrossRef](#)]
103. Tian, Y.; Tomus, D.; Rometsch, P.; Wu, X. Influences of processing parameters on surface roughness of Hastelloy X produced by selective laser melting. *Addit. Manuf.* **2017**, *13*, 103–112. [[CrossRef](#)]
104. Tangsopha, W.; Thongsri, J.; Busayaporn, W. Simulation of ultrasonic cleaning and ways to improve the efficiency. In Proceedings of the 5th International Electrical Engineering Congress, Pattaya, Thailand, 8–10 March 2017; IEEE345: New York, NY, USA, 2017.
105. Fatyukhin, D.S.; Nigmatzyanov, R.L.; Prikhodko, V.M.; Sukhov, A.V.; Sundukov, S.K. A Comparison of the Effects of Ultrasonic Cavitation on the Surfaces of 45 and 40Kh Steels. *Metals* **2022**, *12*, 138. [[CrossRef](#)]
106. Gavrilov, N.V.; Mesyats, G.A.; Nikulin, S.P.; Radkovskii, G.V.; Elkind, A.; Perry, A.J.; Treglio, J.R. New broad beam gas ion source for industrial application. *J. Vac. Sci. Technol. A* **1996**, *14*, 1050–1055. [[CrossRef](#)]
107. Kolikov, V.; Bogomaz, A.; Budin, A. *Powerful Pulsed Plasma Generators: Research and Application*; Springer: Cham, Switzerland, 2018; Introduction Chapter; pp. 1–12.
108. Walton, S.G.; Cothran, C.D.; Amatucci, W.E. Electron Beam Propagation in Magnetic Fields. *IEEE Trans. Plasma Sci.* **2011**, *39*, 2574–2575. [[CrossRef](#)]
109. Yu, Y.C.; Bai, S.; Wang, S.T.; Hu, A.M. Ultra-Short Pulsed Laser Manufacturing and Surface Processing of Microdevices. *Engineering* **2018**, *4*, 779–786. [[CrossRef](#)]
110. Korkmaz, K.; Ribalko, A.V. Effect of pulse shape and energy on the surface roughness and mass transfer in the electrospark coating process. *Kov. Mater. Met. Mater.* **2011**, *49*, 265–270. [[CrossRef](#)]
111. Feng, S.; Xia, M.; Ge, C.C. Consecutive induction melting of nickel-based superalloy in electrode induction gas atomization. *Chin. Phys. Soc.* **2017**, *26*, 6. [[CrossRef](#)]
112. Antonov, D.; Strizhak, P. Explosive Disintegration of Two-Component Droplets in a Gas-Flow at Its Turbulization. *Therm. Sci.* **2019**, *23*, 2983–2993. [[CrossRef](#)]
113. Ivanov, Y.F.; Lopatin, I.V.; Petrikova, E.A.; Rygina, M.E.; Tolkachev, O.S.; Shimanskii, V.I. Structure and Properties of Silumin Surface after Vacuum Arc Plasma-Assisted Deposition of Coatings Irradiated by Low Energy High Current Pulsed Electron Beam. *Russ. Phys. J.* **2020**, *62*, 2106–2111. [[CrossRef](#)]

114. Bardos, L.; Barankova, H. Cold atmospheric plasma: Sources, processes, and applications. *Thin Solid Film.* **2010**, *518*, 6705–6713. [[CrossRef](#)]
115. Jiang, S.; Qiu, L.W.; Li, Z.; Zhang, L.; Rao, J.F. A New All-Solid-State Bipolar High-Voltage Multilevel Generator for Dielectric Barrier Discharge. *IEEE Trans. Plasma Sci.* **2020**, *48*, 1076–1081. [[CrossRef](#)]
116. Tatar, N.; Tuzlah, M.; Bahce, E. Investigation of the Lattice Production of Removable Dental Prostheses with CoCr Alloy Using Additive Manufacturing. *J. Mater. Eng. Perform.* **2021**, *30*, 6722–6731. [[CrossRef](#)]
117. Navinsek, B.; Panjan, P.; Milosev, I. PVD coatings as an environmentally clean alternative to electroplating and electroless processes. *Surf. Coat. Technol.* **1999**, *116*, 476–487. [[CrossRef](#)]
118. Kovalenko, V.A. Use of the vacuum arc discharge for the surface modification. *Fundam. Mech. Low-Energy-Beam-Modif. Surf. Growth Process.* **2000**, *585*, 129–134. [[CrossRef](#)]
119. Kikuchi, E.; Kikuchi, Y.; Hirao, M. Monitoring and Analysis of Solvent Emissions from Metal Cleaning Processes for Practical Process Improvement. *Ann. Occup. Hyg.* **2012**, *56*, 829–842. [[PubMed](#)]
120. Yoon, S.S.; Khang, D.Y. Facile and Clean Release of Vertical Si Nanowires by Wet Chemical Etching Based on Alkali Hydroxides. *Small* **2013**, *9*, 905–912. [[CrossRef](#)]
121. Razab, M.K.A.A.; Noor, A.M.; Jaafar, M.S.; Abdullah, N.H.; Suhaimi, F.M.; Mohamed, M.; Adam, N.; Yusuf, N.A.A.N. A review of incorporating Nd:YAG laser cleaning principal in automotive industry. *J. Radiat. Res. Appl. Sci.* **2018**, *11*, 393–402. [[CrossRef](#)]
122. Kuznetsov, A.P.; Buzinskij, O.I.; Gubsky, K.L.; Nikitina, E.A.; Savchenkov, A.V.; Tarasov, B.A.; Tugarinov, S.N. Development of a laser cleaning method for the first mirror surface of the charge exchange recombination spectroscopy diagnostics on ITER. *Phys. At. Nucl.* **2015**, *78*, 1677–1685. [[CrossRef](#)]
123. Metel, A.; Grigoriev, S.; Volosova, M.; Melnik, Y.; Mustafaev, E. Synthesis of aluminum nitride coatings assisted by fast argon atoms in a magnetron sputtering system with a separate input of argon and nitrogen. *Surf. Coat. Technol.* **2020**, *398*, 126078. [[CrossRef](#)]
124. Mizerov, A.M.; Timoshnev, S.N.; Nikitina, E.V.; Sobolev, M.S.; Shubin, K.Y.; Berezovskaia, T.N.; Mokhov, D.V.; Lundin, W.V.; Nikolaev, A.E.; Bouravleuv, A.D. On the Specific Features of the Plasma-Assisted MBE Synthesis of n^+ -GaN Layers on GaN/c-Al₂O₃ Templates. *Semiconductors* **2019**, *53*, 1187–1191. [[CrossRef](#)]
125. Kamensky, E. Digital technologies in the Russians' everyday life: Analysis based on the opinion surveys. *Ann. XXI* **2020**, *186*, 134–142. [[CrossRef](#)]
126. Dai, Y.; Zhang, M.; Li, Q.; Wen, L.; Wang, H.; Chu, J. Separated Type Atmospheric Pressure Plasma Microjets Array for Maskless Microscale Etching. *Micromachines* **2017**, *8*, 173. [[CrossRef](#)]
127. Su, X.; Ji, C.; Xu, Y.; Li, D.; Walker, D.; Yu, G.; Li, H.; Wang, B. Surface Texture Evolution of Fused Silica in a Combined Process of Atmospheric Pressure Plasma Processing and Bonnet Polishing. *Coatings* **2019**, *9*, 676. [[CrossRef](#)]
128. Yen, T.; Chin, A.; Gritsenko, V. High Performance All Nonmetal SiN_x Resistive Random Access Memory with Strong Process Dependence. *Sci. Rep.* **2020**, *10*, 2807. [[CrossRef](#)] [[PubMed](#)]
129. Solovyev, A.A.; Lebedynskiy, A.M.; Shipilova, A.V.; Ionov, I.V.; Smolyanskiy, E.A.; Lauk, A.L.; Remnev, G.E.; Maslov, A.S. Scale-up of Solid Oxide Fuel Cells with Magnetron Sputtered Electrolyte. *Fuel Cells* **2017**, *17*, 378–382. [[CrossRef](#)]
130. Zolotukhin, D.B.; Oks, E.M.; Tyunkov, A.V.; Yakovlev, E.V.; Yushkov, Y.G. Effect of a dielectric cavity on the ion etching of dielectrics by electron beam-produced plasma generated by a forevacuum plasma electron source. *Vacuum* **2021**, *192*, 110483. [[CrossRef](#)]
131. Marinov, D.; de Marneffe, J.F.; Smets, Q.; Arutchelvan, G.; Bal, K.M.; Voronina, E.; Rakhimova, T.; Mankelevich, Y.; El Kazzi, S.; Mehta, A.N.; et al. Reactive plasma cleaning and restoration of transition metal dichalcogenide monolayers. *NPJ 2D Mater. Appl.* **2021**, *5*, 17. [[CrossRef](#)]
132. Rakhimberlinova, Z.B.; Takibayeva, A.T.; Nazarova, O.G.; Iskakov, A.R.; Musina, G.N.; Kulakov, I.V. Activation Method of Cleaning Process Gas. *News Natl. Acad. Sci. Repub. Kazakhstan Ser. Chem. Technol.* **2020**, *3*, 73–79. [[CrossRef](#)]
133. Vizir, A.V.; Oks, E.M.; Yushkov, G.Y. Broad-beam high-current DC ion source based on a two-stage glow discharge plasma. *Rev. Sci. Instrum.* **2010**, *81*, 02B304. [[CrossRef](#)]
134. Gusev, V.V.; Dolgoplov, V.M.; Slovetskii, D.I.; Shelykhmanov, E.F. Spectral Features of a Hf Discharge Plasma in Etching Aluminum. *High Temp.* **1983**, *21*, 19–25.
135. Yang, S.Y.; Abelson, J.R. Amorphous-Silicon Alloys on C-Si-Influence of Substrate Cleaning and Ion-Bombardment on Film Adhesion and Microstructure. *J. Vac. Sci. Technol. A Vac. Surf. Film.* **1993**, *11*, 1327–1331. [[CrossRef](#)]
136. Ye, C.; Xu, Y.J.; Huang, X.J.; Ning, Z.Y. Effect of high-frequency on etching of SiCOH films in CHF₃ dual-frequency capacitively coupled plasmas. *Thin Solid Film.* **2010**, *518*, 3223–3227. [[CrossRef](#)]
137. Denisov, V.V.; Akhmadeev, Y.H.; Koval, N.N.; Kovalsky, S.S.; Lopatin, I.V.; Ostroverkhov, E.V.; Pedin, N.N.; Yakovlev, V.V.; Schanin, P.M. The source of volume beam-plasma formations based on a high-current non-self-sustained glow discharge with a large hollow cathode. *Phys. Plasmas* **2019**, *26*, 123510. [[CrossRef](#)]
138. Lopatin, I.V.; Schanin, P.M.; Akhmadeev, Y.H.; Kovalsky, S.S.; Koval, N.N. Self-sustained low pressure glow discharge with a hollow cathode at currents of tens of amperes. *Plasma Phys. Rep.* **2012**, *38*, 585–589. [[CrossRef](#)]
139. Li, T.J.; Cui, S.H.; Liu, L.L.; Li, X.Y.; Wu, Z.C.; Ma, Z.Y.; Fu, R.K.Y.; Tian, X.B.; Chu, P.K.; Wu, Z.Z. Magnetic field optimization and high-power discharge characteristics of cylindrical sputtering cathode. *Acta Phys. Sin.* **2021**, *70*, 045202.

140. Raoux, S.; Tanaka, T.; Bhan, M.; Ponnkantti, H.; Seamons, M.; Deacon, T.; Xia, L.Q.; Pham, F.; Silveti, D.; Cheung, D.; et al. Remote microwave plasma source for cleaning chemical vapor deposition chambers: Technology for reducing global warming gas emissions. *J. Vac. Sci. Technol. B* **1999**, *17*, 477–485. [[CrossRef](#)]
141. Watanabe, Y.; Elliott, S.; Firsov, A.; Hout, A.; Leonov, S. Rapid control of force/momentum on a model ramp by quasi-DC plasma. *J. Phys. D Appl. Phys.* **2019**, *52*, 444003. [[CrossRef](#)]
142. Jiang, N.; Ji, A.L.; Cao, Z.X. Atmospheric pressure plasma jet: Effect of electrode configuration, discharge behavior, and its formation mechanism. *J. Appl. Phys.* **2009**, *106*, 013308. [[CrossRef](#)]
143. Sosnin, E.A.; Goltsova, P.A.; Panarin, V.A.; Skakun, V.S.; Tarasenko, V.F.; Didenko, M.V. Formation of Nitrogen Oxides in an Apokamp-Type Plasma Source. *Russ. Phys. J.* **2017**, *60*, 701–705. [[CrossRef](#)]
144. Es'kin, V.A.; Kudrin, A.V. Stationary Structure of a High-Frequency Discharge Maintained by a Distributed Electromagnetic Source in the Presence of an External Magnetic Field. *J. Exp. Theor. Phys.* **2010**, *110*, 701–709. [[CrossRef](#)]
145. Sun, D.L.; Hong, R.Y.; Wang, F.; Liu, J.Y.; Kumar, M.R. Synthesis and modification of carbon nanomaterials via AC arc and dielectric barrier discharge plasma. *Chem. Eng. J.* **2016**, *283*, 9–20. [[CrossRef](#)]
146. Kim, J.; Kim, S.-j.; Lee, Y.-N.; Kim, I.-T.; Cho, G. Discharge Characteristics and Plasma Erosion of Various Dielectric Materials in the Dielectric Barrier Discharges. *Appl. Sci.* **2018**, *8*, 1294. [[CrossRef](#)]
147. Li, Z.; Shi, Z.W.; Sun, Q.J.; Wei, C.Y.; Geng, X. Analysis of flow separation control using nanosecond-pulse discharge plasma actuators on a flying wing. *Plasma Sci. Technol.* **2018**, *20*, 115504. [[CrossRef](#)]
148. Nguyen, D.S.; Park, H.S.; Lee, C.M. Effect of cleaning gas stream on products in selective laser melting. *Mater. Manuf. Process.* **2019**, *34*, 455–461. [[CrossRef](#)]
149. Gabdrakhmanov, A.T.; Israphilov, I.H.; Shafigullin, L.N. The metal surface cleaning using a vapor-gas discharge. *IOP Conf. Ser. J. Phys. Conf. Ser.* **2018**, *1058*, 012009. [[CrossRef](#)]
150. Bolotov, M.G.; Prybytko, I.O. Application of Glow Discharge Plasma for Cleaning (Activation) and Modification of Metal Surfaces while Welding, Brazing, and Coating Deposition. *Prog. Phys. Met.* **2021**, *22*, 103–128. [[CrossRef](#)]
151. Sosnin, E.A.; Panarin, V.A.; Skakun, V.S.; Tarasenko, V.F.; Pechenitsyn, D.S.; Kuznetsov, V.S. Source of an atmospheric-pressure plasma jet formed in air or nitrogen under barrier discharge excitation. *Tech. Phys.* **2016**, *61*, 789–792. [[CrossRef](#)]
152. Rao, J.F.; Liu, K.F.; Qiu, J. An Efficient All Solid-State Pulsed Generator for Pulsed Discharges. In Proceedings of the 2012 IEEE International Power Modulator and High Voltage Conference, San Diego, CA, USA, 3–7 June 2012; pp. 473–476.
153. Bocharnikov, V.M.; Volodin, V.V.; Golub, V.V.; Trifanov, I.V.; Serebryakov, D.G. Resonance Properties of a Low-Pressure Dielectric Barrier Discharge. *Tech. Phys.* **2020**, *65*, 1969–1974. [[CrossRef](#)]
154. Tao, X.P.; Lu, R.D.; Li, H. Electrical Characteristics of Dielectric-Barrier Discharges in Atmospheric Pressure Air Using a Power-Frequency Voltage Source. *Plasma Sci. Technol.* **2012**, *14*, 723–727. [[CrossRef](#)]
155. Erofeev, M.; Baksht, E.; Tarasenko, V. Miniaturized ultraviolet sources driven by dielectric barrier discharge and runaway electron preionized diffuse discharge. *Opt. Appl.* **2014**, *44*, 475–487.
156. Yang, L.Z.; Liu, Z.W.; Mao, Z.G.; Li, S.; Chen, Q. Formation and characteristics of patterns in atmospheric-pressure radio-frequency dielectric barrier discharge plasma. *Jpn. J. Appl. Phys.* **2017**, *56*, 01AC02. [[CrossRef](#)]
157. Brandenburg, R. Dielectric barrier discharges: Progress on plasma sources and on the understanding of regimes and single filaments. *Plasma Sources Sci. Technol.* **2018**, *27*, 079501. [[CrossRef](#)]
158. Timshina, M.; Eliseev, S.; Kalinin, N.; Letunovskaya, M.; Burtsev, V. Numerical investigation of dynamics and gas pressure effects in a nanosecond capillary sliding discharge. *J. Appl. Phys.* **2019**, *125*, 143302. [[CrossRef](#)]
159. Samaei, A.; Chaudhuri, S. Multiphysics modeling of metal surface cleaning using atmospheric pressure plasma. *J. Appl. Phys.* **2020**, *128*, 054903. [[CrossRef](#)]
160. Nasreen, A.; Shaker, K.; Nawab, Y. Effect of surface treatments on metal–composite adhesive bonding for high-performance structures: An overview. *Compos. Interfaces* **2021**, *28*, 1221–1256. [[CrossRef](#)]
161. Kuznetsov, V.S.; Sosnin, E.A.; Panarin, V.A.; Skakun, V.S.; Pechenitsyn, D.S.; Tarasenko, V.F. Observation of Streamer Coronas Preceding the Formation of an Apokampic Discharge. *Russ. Phys. J.* **2019**, *62*, 992–995. [[CrossRef](#)]
162. Emel'yanov, A.A.; Plotnikov, M.Y.; Rebrov, A.K.; Timoshenko, N.I.; Yudin, I.B. The Use of a Supersonic Jet of Gas Activated in a Microwave Discharge in Diamond Deposition. *Fluid Dyn.* **2021**, *56*, 106–115. [[CrossRef](#)]
163. Zorin, V.G.; Lazebnik, B.S.; Lunin, N.V.; Markov, G.A. Resonance Super-High Frequency Discharge in a Magnetic-Field. *Zhurnal Tekhnicheskoi Fiz.* **1975**, *45*, 1006–1009.